*J. Fluid Mech.* (1998), *vol.* 375, *pp.* 265–296. Printed in the United Kingdom

© 1998 Cambridge University Press

# Motion of a sphere near planar confining boundaries in a Brinkman medium

By J. FENG, P. GANATOS AND S. WEINBAUM†

Department of Mechanical Engineering, The City College of the City University of New York, New York, NY 10031, USA

(Received 14 July 1997 and in revised form 22 June 1998)

A general numerical method using the boundary integral equation technique of Pozrikidis (1994) for Stokes flow in an axisymmetric domain is used to obtain the first solutions to the Brinkman equation for the motion of a particle in the presence of planar confining boundaries. The method is first applied to study the perpendicular and parallel motion of a sphere in a fibre-filled medium bounded by either a solid wall or a planar free surface which remains undeformed. By accurately evaluating the singular integrals arising from the discretization of the resulting integral equation, one can efficiently and accurately treat flow problems with high $\alpha$ defined by $r_s/K_p^{1/2}$ in which $r_s$ is the radius of the sphere and $K_p$ is the Darcy permeability. Convergence and accuracy of the new technique are tested by comparing results for the drag with the solutions of Kim & Russell (1985*a*) for the motion of two spheres perpendicular to their line of centres in a Brinkman medium. Numerical results for the drag and torque exerted on the particle moving either perpendicular or parallel to a confining planar boundary are presented for $\epsilon \geqslant 0.1$, in which $\epsilon r_s$ is the gap between the particle and the boundary. When the gap width is much smaller than $r_s$, a local analysis using stretched variables for motion of a sphere indicates that the leading singular term for both drag and torque is independent of $\alpha$ provided that $\alpha = O(1)$. These results are of interest in modelling the penetration of the endothelial surface glycocalyx by microvilli on rolling neutrophils and the motion of colloidal gold and latex particles when they are attached to membrane receptors and observed in nanovid (video enhanced) microscopy. The method is then applied to investigate the motion of a sphere translating in a channel. The drag and torque exerted on the sphere are obtained for various values of $\alpha$, the channel height $H$ and particle position $b$. These numerical results are used to describe the diffusion of a spherical solute molecule in a parallel walled channel filled with a periodic array of cylindrical fibres and to assess the accuracy of a simple multiplicative formula proposed in Weinbaum *et al.* (1992) for diffusion of a solute in the interendothelial cleft.

## 1. Introduction

The motion of a particle in a porous material adjacent to confining boundaries is of interest most notably in the areas of chemical and biomedical engineering and the biophysics of membranes. The motivation for the present study stems from several recent developments in the study of thin surface layers of matrix that coat the

† Author to whom correspondence should be addressed: e-mail weinbaum@med2s0.engr.ccny.cuny.edu.

membranes of living cells (Weinbaum 1998). Of particular interest is the thin polyelectrolyte layer of loose fibres that form the surface glycocalyx, literally 'sugar coat', of endothelial cells and the possible extension of this matrix into the interendothelial clefts, the 20 nm wide extracellular channel between endothelial cells through which water and solutes cross the capillary wall (Weinbaum, Tsay & Curry 1992; Fu, Curry & Weinbaum 1994). This surface glycocalyx, which has been estimated to be from 100 nm (Adamson & Clough 1992) to 400 nm thick (Vink & Duling 1996) using electron and fluorescence microscopy, is the principal sieving layer for plasma proteins that determines the colloidal osmotic force across the capillary wall. This surface coat is also thought to play a major role in receptor–ligand interactions between the tips of microvilli in the rolling interaction of neutrophils on the endothelial surface (Bruehl, Springer & Bainton 1996; Alon *et al.* 1997) and single particle tracking (SPT) experiments where 20 to 40 nm colloidal gold and larger latex and polystyrene beads up to 200 nm diameter are attached to membrane receptor molecules and observed in nanovid (video enhanced) microscopy. The latter experiments have been used to estimate pericellular matrix viscosity (Lee *et al.* 1993), to explore the surface dynamics of transmembrane integrins in migrating fibroblasts (Schmidt *et al.* 1993), to elucidate the structure of the submembrane actin cytoskeleton (Sako & Kusumi 1995) and to study the movement of cell-cell adhesion molecules (Sako *et al.* 1998) to mention just a few of the numerous studies in this rapidly growing field. In many of these studies, picoNewton forces generated by optical gradient traps (laser tweezers) are used to drag gold and latex tagged membrane proteins laterally in the plane of the membrane against the combined resistance of the cytoskeleton, the membrane lipid and the extracellular matrix.

In this paper an effective-medium theory based on the Brinkman equation will be developed to examine the motion of particles in a porous medium in the presence of one or more confining boundaries. In particular, we shall be interested in (i) the perpendicular motion of a sphere near a fibre-coated planar wall as a simple idealized model for calculating the hydrodynamic interaction of a microvilli tip with the endothelial surface glycocalyx, (ii) the translational motion of a sphere parallel to a fibre-coated planar wall as a model for calculating the hydrodynamic resistance of the gold and latex particles in the surface glycocalyx or the lateral diffusion of a solute molecule in the layer, and (iii) the motion of a sphere in a fibre-filled channel as a model for solutes diffusing through the interendothelial cleft. The latter model is also of interest in investigating the transport of lipoproteins in the thin layer of intimal matrix between the endothelial cells and the internal elastic lamina of arteries and the growth of cellular level macromolecular leakage spots (Huang *et al.* 1994). In the problems involving molecular diffusion we shall assume that the diffusing molecule is smaller than the open gap $\Delta$ between the matrix fibres, which is taken to be 7 nm, the effective diameter of albumin, the most abundant plasma protein. The value of $\Delta$ would permit the surface glycocalyx to serve as the molecular filler or barrier that establishes the oncotic force for plasma proteins across capillary endothelium (Weinbaum 1998). As we shall discuss shortly, this value of $\Delta$ will place a constraint on the maximum value of the permeability parameter $\alpha$ that appears in the Brinkman equation. For problems involving gold and latex tracer particles this estimated fibre spacing will be 3 to 30 times smaller than the test sphere that is dragged through the surface matrix. In this case one must also consider the elastic and binding energy stored in the fibres. A rough estimate of the relative magnitude of the hydrodynamic and these other effects can be obtained by calculating the hydrodynamic resistance due to the fibres and subtracting it from the total drag on the particles estimated from their diffusional mobility.

The Brinkman (1947) equation has been widely used in calculating the hydrodynamic interaction and hindered transport of solid spherical particles in ordered or disordered fibrous media. Since the Brinkman equation has only one additional parameter, $K_p$, which characterizes the permeability of the porous media, one does not have to have a knowledge of the detailed structure of the porous media once the permeability has been determined either by theoretical prediction or experimental measurement. When the equation is scaled by the particle radius $r_s$ and made dimensionless a single parameter, $\alpha = r_s/K_p^{1/2}$, appears: $\alpha$ describes the ratio of the particle dimension to the fibre interaction layer thickness, $K_p^{1/2}$; $K_p$ in turn depends on the fibre spacing $\Delta$ and to a lesser extent on the fibre radius $a$. The analysis in Tsay & Weinbaum (1991) shows that $K_p^{1/2}$ is of the same order as the fibre spacing $\Delta$.

A central issue in using the Brinkman equation to describe the drag and torque exerted on a diffusing particle is the limitation on $\alpha$ for which the effective-medium theory applies. This parameter describes the transition from small-scale viscous motion described by the Stokes equation to larger-scale pressure-driven motions governed by Darcy's law. To address this question, Durlofsky & Brady (1987) first compared the Green's function (point force) for the Brinkman equation with the solution for a point force using a Stokesian dynamic simulation for a point force in a periodic particle array. It was found that the Green's function in effective-medium theory accurately describes the Stokes flow in the near field and the dipole flow in the far field provided the solid fraction is less than 5 %. Phillips, Deen & Brady (1989, 1990) subsequently employed a Stokesian dynamic simulation in which they represented the fibres as either parallel strands of spherical beads or cylinders and examined the motion of a test sphere relative to an ordered strand array. They concluded that in the low fibre fraction limit, the far field interaction between the mobile particle and the fibres dominates the contribution arising from the local inhomogeneity of the medium due to the existence of the particle. The effective-medium theory was most accurate in the dilute fibre limit, fibre fraction less than 5 %, where the value of $\alpha$ was less than $O(1)$ and the particle was small compared to the fibre spacing. They also found that the diffusivity calculated from the Brinkman equation agrees quite well with that obtained by the more rigorous Stokesian dynamic method, provided steric effects are included. The same conclusion is reached in figure 10 of the present study, where we demonstrate using the steric exclusion theory in Tsay & Weinbaum (1991) for a periodic fibre array, that good agreement can be obtained with Stokesian dynamic simulations when the fibre fraction is $\leqslant 0.1$. Experimental results for the diffusivity of a macromolecule in a fibrous gel also indicate that the Brinkman equation is a good model, in particular for a medium with low fibre volume fraction (Johnson *et al.* 1996). Moreover, Kosar & Phillips (1995) have shown that the Brinkman model for describing screened hydrodynamic interactions gives results equivalent to models of the Kirkwood–Riseman type, in which the effects of the fixed fibres are modelled using a distribution of immobile point forces. All of the aforementioned work seems to support the contention that the application of the Brinkman medium model may be limited more by an inadequate knowledge of the actual microstructure than by any inherent limitations in the effective-medium approach when the fibre fraction is small.

In the past, several investigators have attempted to derive the Brinkman equation using various models for Stokes flow in unbounded porous media. Tam (1969) averaged the Stokes equation governing slow viscous flow past a cloud of spherical particles. This approach led to a Brinkman equation and thus provided a more rigorous theoretical basis for its application. The uncertainty in the definition of the

viscosity in the Brinkman equation in Tam's method was examined more thoroughly by Lundgren (1972), who extended Tam's method to both stationary beds and suspensions of particles. Howells (1974) developed an iterative scheme for obtaining the average drag for flow through random arrays of either spheres or parallel circular posts at small solid fraction. More recently, the Brinkman equation has also been examined for flow in a bounded medium composed of a perpendicular periodic array of circular cylindrical fibres in a parallel walled channel (Tsay & Weinbaum 1991). It was shown that very good agreement with the Stokes solution for the flow through the fibres in the channel could be obtained by solving the Brinkman equation for all values of $\alpha = h/K_p^{1/2}$, where $h$ is here the channel height, provided that the aspect ratio of the fibres was greater than five. Furthermore, good agreement for the drag could be obtained for all fibre volume fractions when $K_p$ was described by its expression for a two-dimensional unbounded fibre array.

Although various solution techniques have been developed for treating the motion of a sphere in Stokes flow in the presence of boundaries, there are no prior solutions to the Brinkman equation for the motion of a sphere in a bounded medium. The general solution of the Brinkman equation involves three scalar functions obtained by solving a Laplace equation and two modified Helmholtz equations (Kim & Russel 1985*a*). These solutions are analogous to the harmonic functions for creeping flow. Since the Helmholtz equation admits fewer separable solutions than the Laplace equation in various orthogonal coordinate systems, such as bipolar and toroidal coordinates, solutions for the hydrodynamic interaction between particles or a particle and confining boundaries in a Brinkman medium are very limited. One solution of the Brinkman equation of particular interest in evaluating the accuracy of the numerical solution technique developed herein is the interaction between two spherical particles. This problem was investigated by Kim & Russel (1985*a*) to determine the effect of pair interactions on the effective permeability and viscosity of an array of fixed particles (Kim & Russel 1985*b*). These authors used the method of reflections for weak interactions in which the particles were far removed from each other, or the boundary collocation technique of Gluckman, Pfeffer & Weinbaum (1971) for strong interactions in which the clearance between the particles was comparable to their diameter.

The boundary integral equation method has been widely used in creeping flow problems since it was first introduced by Youngren & Acrivos (1975). This numerical method is computationally efficient and flexible in treating both rigid and deformable flow geometries. Great progress has been made over the past twenty years in improving its accuracy and reducing computational efforts, especially in the special treatment of the singular integral which arises in the calculation of the contribution from the element containing the collocation point and in reducing the dimensions of the problem for special flow configurations. In addition to the traditional formulation, in which one reduces the flow problem to solving a system of Fredholm integral equations of the first kind for the surface traction defined on the surfaces of all boundaries in the flow field, alternative formulations leading to integral equations of the second kind have also been developed to treat multiple particles. Green's functions that satisfy the no-slip boundary conditions on infinite boundaries have also been used to obtain several Stokes solutions for the motion of spheres, spheroids and slender objects moving near walls (Weinbaum, Ganatos & Yan 1990). These fundamental solutions for bounded flow are available for only a few flow geometries. No such Green's functions are known for the Brinkman equation.

In contrast to Stokes flows, where the drag on a particle is the same whether the

particle is moving in a stationary fluid at infinity or there is a uniform flow past a stationary particle, in a Brinkman medium these two solutions are not interchangeable since for a uniform flow there is a finite pressure gradient at infinity described by the Darcy resistance. This gives rise to a term which is proportional to the volume of the particle. The second fundamental difference is that the Darcy permeability $K_p$ is a function of the fibre spacing and fibre radius, and not all values of $K_p$ are permissible unless the fibres are highly flexible. A sphere of radius $r_s$ will not be able to translate in a rigid periodic fibre array when the open spacing between fibres, $\Delta$, is less than the sphere diameter. Thus for a rigid fibre array, the Brinkman parameter $\alpha = r_s/K_p^{1/2}$ describing the motion of a spherical particle in a Brinkman medium will have a maximum value if the particle is not to be trapped by the fibres. For a periodic fibre array one must satisfy a complementary constraint on $K_p$ that $\Delta > 2r_s$. Curiously, this fundamental constraint does not appear to have been examined previously in the literature. For a spherical particle diffusing in a rigid fibre array, we shall show that this maximum value of $\alpha$ is approximately 1.5 and varies weakly with the fibre radius. This limitation on $\alpha$ will not apply if a large particle is forcibly moved through a highly flexible matrix with weak fibre adhesion energy. This would appear to be the case when a large tracer particle is dragged by optical tweezers through a surface glycocalyx or when a microvilli on a white cell penetrates this surface layer. In these applications our theory only describes the hydrodynamic resistance of these motions and not the elastic and adhesion energy of the fibres. $\alpha$ in these applications can be $O(10)$ or larger.

In the present work, we shall take advantage of the axisymmetry of the boundaries using a technique developed by Pozrikidis (1994) for Stokes flows. This allows us to decompose all the flow variables into a complex Fourier series with respect to the common azimuthal angle. The original three-dimensional integral equation is thereby reduced to a set of one-dimensional integral equations defined on the contours of the boundaries. Further simplification is achieved by considering the fact that only the first-order harmonics need be retained for translation and the corresponding double layer contribution can be evaluated analytically. A standard boundary collocation technique is used to discretize the boundary contours into small segments. By using a numerical technique that can accurately calculate the singular integrals, we can also apply our method to flows in porous media of small permeability, $\alpha \gg 1$. This removes a technical difficulty of the boundary integral equation method for flows governed by the Brinkman equation, or the mathematically equivalent unsteady creeping flow equations (Pozrikidis 1988; Loewenberg 1994).

The method is then used to calculate the drag and torque coefficients for a sphere translating in a fibrous medium in a channel. These solutions illustrate the relative importance of shielding by the walls compared to shielding by the fibres. The solutions are then used as input into a Stokes–Einstein model for determining the diffusion coefficient for a spherical particle in a fibre-filled channel. A new hydrodynamic theory for determining the approximate diffusive permeability of a spherical molecule in an inter-endothelial cleft, our initial motivation for this work, is presented as an application of the numerical results. The theory also takes steric exclusion into consideration. Comparison with a previously obtained simple multiplicative formula for the diffusive permeability in which the effects of the fibre matrix and the walls were treated separately (Weinbaum *et al.* 1992) reveals that the earlier approximate method provides an underestimation of the diffusive permeability. A brief discussion of the present method and further applications in creeping flows conclude the paper.

## 2. Boundary integral formulation for flow in a Brinkman medium

The Brinkman (1947) equation,

$$\nabla p = \mu \nabla^2 \boldsymbol{v} - \frac{\mu}{K_p} \boldsymbol{v}, \tag{2.1}$$

together with the continuity equation for an incompressible viscous fluid,

$$\nabla \cdot \boldsymbol{v} = 0. \tag{2.2}$$

are often used to describe flows in porous media in which the pressure gradient, velocity gradient and Darcy resistance are of comparable importance. As previously noted by Kim & Russel (1985*a*), the solution of equation (2.1) for the velocity field can be expressed by three scalar functions which satisfy Laplace's equation and two Helmholtz equations. However, the Helmholtz equation does not permit solutions by separation of variables in bispherical coordinates. This makes it difficult to study the motion of a sphere in the proximity of an infinite wall. In this section, a general boundary integral equation method will be formulated in order to investigate bounded flow problems such as particle motion near a planar boundary or between two parallel walls. The complexity of the resulting integral equations usually precludes analytical solution so that solutions must be obtained by numerical methods. A simple effective and flexible collocation boundary element discretization procedure will be introduced.

We first consider an arbitrary three-dimensional flow problem governed by the Brinkman equation and the continuity equation. Following a procedure similar to that used by Pozrikidis (1994) in treating creeping flow, we write the reciprocal relationship

$$\nabla \cdot (\boldsymbol{u}^* \cdot \boldsymbol{\sigma} - \boldsymbol{u} \cdot \boldsymbol{\sigma}^*) = 0, \tag{2.3}$$

in which $\boldsymbol{u}$ and $\boldsymbol{u}^*$ are any two solutions to the system (2.1) and (2.2), with corresponding stress fields $\boldsymbol{\sigma}$ and $\boldsymbol{\sigma}^*$ at the given point $\boldsymbol{x}$.

The dimensionless Green's function for the Brinkman equation corresponding to the Stokeslet for the creeping flow, is given by

$$S_{ij}(\boldsymbol{x}) = \frac{\delta_{ij}}{r} A + \frac{\hat{x}_i \hat{x}_j}{r^3} B, \tag{2.4}$$

where

$$A = 2\mathrm{e}^{-\alpha r} \left(1 + \frac{1}{\alpha r} + \frac{1}{\alpha^2 r^2}\right) - \frac{2}{\alpha^2 r^2}, \tag{2.5}$$

$$B = -2\mathrm{e}^{-\alpha r} \left(1 + \frac{3}{\alpha r} + \frac{3}{\alpha^2 r^2}\right) + \frac{6}{\alpha^2 r^2}, \tag{2.6}$$

and the associated stress tensor is given by

$$T_{ijk} = \left[\frac{\partial S_{ij}}{\partial \hat{x}_k} + \frac{\partial S_{kj}}{\partial \hat{x}_i}\right] - 2\delta_{ik} \frac{\hat{x}_j}{r^3}. \tag{2.7}$$

Here $\hat{\boldsymbol{x}} = \boldsymbol{x} - \boldsymbol{x}_0$, $r = |\hat{\boldsymbol{x}}|$, and $\delta_{ij}$ is the Kronecker tensor. Now we select a point $\boldsymbol{x}_0$ in the flow domain and integrate the reciprocal relation between the desired solution and above singular solution over the entire control volume composed of the particles, a virtual sphere of infinite radius and a small sphere centred at the singular point. Using the divergence theorem in conjunction with the asymptotic properties of the singular solutions at infinity, and applying the result for a point on the surface of arbitrary solid boundaries, one can express the velocity field in terms of a boundary

integral equation

$$u_j(\boldsymbol{x}_0) = -\frac{1}{4\pi\mu}\int_{S_p}[f_i(\boldsymbol{x})S_{ij}(\hat{\boldsymbol{x}}) - u_i(\boldsymbol{x})T_{ijk}(\hat{\boldsymbol{x}})\boldsymbol{n}_k(\boldsymbol{x})]\mathrm{d}S(\boldsymbol{x}), \tag{2.8}$$

where $\boldsymbol{f} = \boldsymbol{\sigma}\cdot\boldsymbol{n}$, $S_p$ denotes the entire boundary including the particle surfaces, with $\boldsymbol{n}$ being the unit normal vector pointing into the fluid.

Equation (2.8) is applicable to particle motion in a Brinkman medium with or without any other confining boundaries. In deriving this equation, we have assumed that the velocity decays at infinity at a sufficiently fast rate. Otherwise, it must be applied to an appropriately chosen disturbance flow field which satisfies asymptotically decaying conditions. For example, for uniform pressure-driven flow in an otherwise quiescent Brinkman medium, we can separate the contribution to the total velocity into the flow at infinity plus the integral in (2.8)

$$u_j(\boldsymbol{x}_0) = u_{j\infty}(\boldsymbol{x}) - \frac{1}{4\pi\mu}\int_{S_p}[f_i(\boldsymbol{x})S_{ij}(\hat{\boldsymbol{x}}) - u_i(\boldsymbol{x})T_{ijk}(\hat{\boldsymbol{x}})\boldsymbol{n}_k(\boldsymbol{x})]\mathrm{d}S(\boldsymbol{x}). \tag{2.9}$$

To this end, we have reduced the problem to a boundary integral equation defined on the surfaces of the boundaries. For a flow problem that involves only the translation of the particle, the second term in the integral in equation (2.8) can be calculated explicitly, i.e. if we define the modified surface traction as $\boldsymbol{f} = \boldsymbol{f}' + \alpha^2(\boldsymbol{v}\cdot\boldsymbol{x})\boldsymbol{n}$, then $\boldsymbol{f}'$ satisfies

$$u_j(\boldsymbol{x}_0) = -\frac{1}{8\pi\mu}\int_{S_p} f_i'(\boldsymbol{x})S_{ij}(\hat{\boldsymbol{x}})\mathrm{d}S(\boldsymbol{x}). \tag{2.10}$$

The total force exerted by the fluid on the particle can be obtained by integrating the surface traction over the entire particle surface. This leads to

$$\int_{S_p}\boldsymbol{f}\mathrm{d}s = \int_{S_p}\boldsymbol{f}'\mathrm{d}s + \alpha^2\boldsymbol{v}V_p \tag{2.11}$$

in which $V_p$ is the volume of the particle.

For uniform flow past stationary particles, it can be verified that $\boldsymbol{f}$ in equation (2.9) is equal to the total surface traction. It does not seem possible to eliminate the associated stress field in (2.8) or (2.10) for the general motion of the particle or for non-uniform upstream flows, as was done by Kim & Karrila (1991) in the creeping flow limit. This difficulty prevents us from obtaining solutions for the rotation of the sphere. Once the integral equations (2.8) or (2.10) are solved for $\boldsymbol{f}$ or $\boldsymbol{f}'$, respectively, the net force and torque exerted on the particle can be readily calculated by integrating $\boldsymbol{f}$ or $\boldsymbol{f}'$ over the entire surface. Starting from the integral equation (2.8), several asymptotic solutions for large or small values of the parameter $\alpha$ can be obtained for the oscillation of a single particle in Stokes flow (Pozrikidis 1988; Loewenberg 1994). These asymptotic solutions can also be applied to the Brinkman equation.

At this point, we focus our attention on a large class of flow problems that are bounded by axisymmetric surfaces, i.e. boundaries generated by rotating the contours about a common $x$-axis in the cylindrical coordinates $(\sigma, \phi, x)$ as illustrated by figure 1. It can be shown that for flows parallel to this axis, the surface traction is a *zeroth*-order harmonic function independent of the azimuthal angle. For the flows perpendicular to this axis, the surface traction is a *first*-order harmonic function of the azimuthal angle $\phi$ (Ganatos, Pfeffer & Weinbaum 1980*b*, Hsu & Ganatos 1991). A more detailed discussion of this issue can be found in Pozrikidis (1992, 1994) for more general axisymmetric boundary conditions.

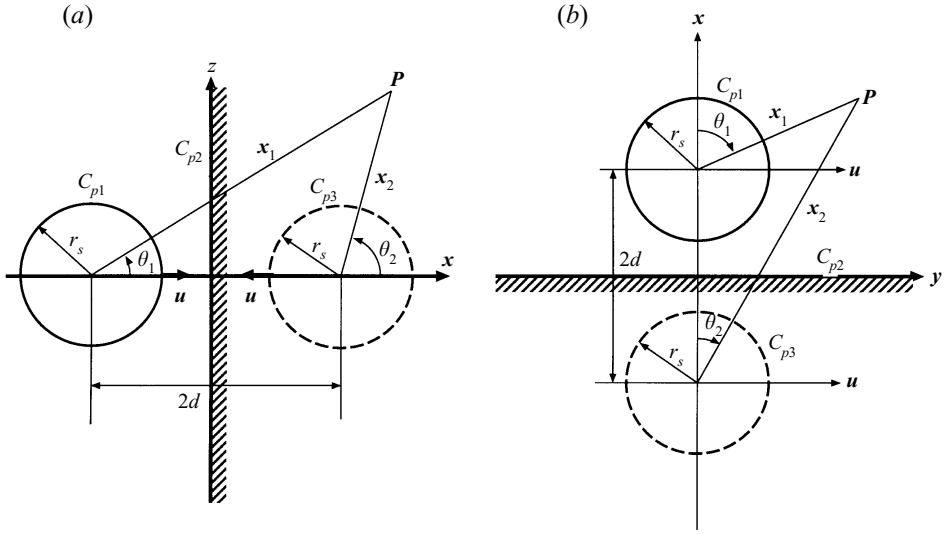


FIGURE 1. Geometry for a sphere translating in the presence of a planar boundary: (*a*) perpendicular motion; (*b*) parallel motion.

Now consider a sphere moving parallel to the axis of rotation $x$ in an axisymmetric domain, figure 1(*a*). In this case, one may perform the integration in the azimuthal direction to reduce the surface integral into a line integral on the contour of each particle and the confining boundaries in a meridional plane. For the translational motion of a sphere along the $x$-axis, the resulting equation will be

$$u_f(\boldsymbol{x}_0) = -\frac{1}{8\pi\mu}\sum_i \int_{C_{pi}} \Psi_{fg}(\boldsymbol{x}, \boldsymbol{x}_0) f'_g(\boldsymbol{x}) \sigma \mathrm{d}l(\boldsymbol{x}), \tag{2.12}$$

where the matrix $\Psi$ is defined as

$$\begin{bmatrix} A_{10} + \hat{x}^2 B_{30} & \hat{x}(\sigma B_{30} - \sigma_0 B_{31}) \\ \hat{x}(\sigma B_{31} - \sigma_0 B_{30}) & A_{11} + (\sigma^2 + \sigma_0^2) B_{31} - \sigma\sigma_0 (B_{30} + B_{32}) \end{bmatrix} \tag{2.13}$$

in which

$$A_{mn} = \int_0^{2\pi} \frac{\cos^n \phi}{r^m} A \mathrm{d}\phi, \qquad B_{mn} = \int_0^{2\pi} \frac{\cos^n \phi}{r^m} B \mathrm{d}\phi. \tag{2.14}$$

Once the surface traction $\boldsymbol{f}$ has been determined from equation (2.12), the drag on the sphere can be obtained by (2.11).

We next consider the motion of a sphere perpendicular to the axis of an axisymmetric domain of the Brinkman medium, figure 1(*b*). We introduce the cylindrical coordinate system $(\sigma, \phi, x)$, decompose the polar cylindrical components of the velocity and surface traction into complex Fourier series with respect to the azimuthal angle, express the integral equation (2.8) or (2.10) also in a complex Fourier series and equate the corresponding components of the boundary conditions of the same order. The linearity of the Fourier series leads to a system of equations relating the Fourier coefficients of the velocity to the boundary surface force. For a sphere translating with the velocity $U_0$, which can be written as a first-order harmonic function dependent upon the azimuthal angle, in the form

$$U_{0x} = U_x \cos\phi, \qquad U_{0\sigma} = U_\sigma \cos\phi, \qquad U_{0\phi} = -U_\phi \sin\phi, \tag{2.15}$$

the Fourier components are $(U_x, U_\sigma, U_\phi) = (0, U_0, U_0)$, whereas for a uniform flow $U^\infty$, these components are $(U_x^\infty, U_\sigma^\infty, U_\phi^\infty) = (0, U^\infty, U^\infty)$. After some tedious evaluation, we obtain the following system of algebraic equations for the unknown Fourier components of the surface traction $\mathscr{F}_g$:

$$U_f(x_0, \sigma_0) = U_f^\infty(x_0, \sigma_0) - \frac{1}{4\pi\mu} \sum_i \int_{C_{pi}} \Phi_{fg}(\hat{x}, \sigma, \sigma_0) \mathscr{F}_g(x, \sigma) \sigma \mathrm{d}l(x). \tag{2.16}$$

Here $\mathrm{d}l(x)$ denotes arclength along the tangent to the surface contour $C_{pi}$ and the kernel $\Phi$ is given by

$$\Phi_{\alpha\beta} = \begin{bmatrix} A_{11} + \hat{x}^2 B_{31} & \hat{x}(\sigma B_{31} - \sigma_0 B_{32}) & \hat{x}\sigma_0(B_{32} - B_{31}) \\ \hat{x}(\sigma B_{32} - \sigma_0 B_{31}) A_{12} + (\sigma^2 + \sigma_0^2) B_{32} - \sigma\sigma_0(B_{33} + B_{31}) & & A_{10} - A_{12} + \sigma_0^2(B_{30} - B_{32}) - \sigma\sigma_0(B_{31} - B_{33}) \\ \hat{x}\sigma(B_{30} - B_{32}) A_{10} - A_{12} + \sigma^2(B_{30} - B_{32}) - \sigma\sigma_0(B_{31} - B_{33}) & & A_{12} + \sigma\sigma_0(B_{31} - B_{33}) \end{bmatrix}, \tag{2.17}$$

and $A_{mn}$, $B_{mn}$ are defined by (2.14).

The relationship between the Fourier components of the surface traction and the actual shear stress $(f_x, f_\sigma, f_\phi)$ is given by

$$(f_x, f_\sigma, f_\phi) = (2\mathscr{F}_x \cos\phi, 2\mathscr{F}_\sigma \cos\phi, -2\mathscr{F}_\phi \sin\phi). \tag{2.18}$$

The components of the force and torque over the boundary $S_{pi}$ are computed by contour integrals along $C_{pi}$, i.e.

$$F_y = 2\pi \int_{C_{pi}} (\mathscr{F}_\sigma + \mathscr{F}_\phi) \sigma \mathrm{d}l(x) \tag{2.19}$$

$$T_z = 2\pi \int_{C_{pi}} [x(\mathscr{F}_\sigma + \mathscr{F}_\phi) - \sigma\mathscr{F}_x] \sigma \mathrm{d}l(x). \tag{2.20}$$

Numerical solution of the integral equations (2.12) and (2.16) is implemented by introducing a standard boundary element collocation technique. First, each part of the boundary contour is discretized by a line segment over which the surface traction $\mathscr{F}$ is assumed to be constant. The boundary elements are non-uniformly distributed in order to resolve the fine structure of the flow field. Typically the size of an element is adjusted smaller in regions where the flow has large gradients. We apply (2.12) or (2.16) at the mid-point of each line segment over all the contours. This yields a system of linear algebraic equations that can be solved by standard reduction methods. The accuracy of the method should improve as the number of elements is increased. Numerical convergence tests and solutions obtained for bounded and unbounded flows will be presented in the results section.

## 3. Evaluation of singular integrals

One of the main difficulties in the boundary integral equation method is the accurate calculation of the singular integrals over the element that includes the collocation point. In this region, the kernel of the integral equation (2.12) and (2.16) exhibits logarithmic singularities. The diagonal components of $\Psi$ in (2.13) and $\Phi$ in (2.17) behave in a singular manner as $\ln(r)$ as $\boldsymbol{x}_0 \to \boldsymbol{x}$ although the off-diagonal components remain regular. Over the past two decades, several techniques

have been suggested to remove this singular part of the numerical quadrature using analytic methods to accurately evaluate the singular contribution. This is critical in the numerical procedure, since the Fredholm integral equation of the first kind suffers numerical instability when an ordinary quadrature scheme is applied. The accurate evaluation of these singular integrals using asymptotic expansions improves the diagonal dominance of the coefficient matrix thereby making it more robust in numerical inversion. However, this subtraction and addition technique only works well for small values of $\alpha$ and will fail for large $\alpha$ (Pozrikidis 1988; Loewenberg 1994).

Recently, Muldowney & Higdon (1995) have suggested a technique which is very effective in solving boundary integral equations for creeping flow problems. This method is based on a transformation of the integrand that clusters quadrature points in the proximity of the singularity. Detailed numerical tests of this method on various singular integrals of the form

$$I = \int_{-1}^{1} \frac{g(s)}{(as^2 + bs + c)^{1/2}} \mathrm{d}s \tag{3.1}$$

in which the denominator of the integrand has a zero on $[-1, 1]$ and $s$ is the parameterized variable, reveal extremely fast convergence and high accuracy with respect to the order of normal Gauss–Legendre quadrature. For brevity, assume a singular point $s_o = 0$ and let $z_i$ denote a standard Gauss–Legendre quadrature point. If we define a mapped variable

$$s_i = \left( \frac{\sinh \beta \xi_i}{\sinh \beta} \right)^2 \tag{3.2}$$

in which $\xi_i = \frac{1}{2}(1 + z_i)$ is the shifted quadrature point and treat $\beta$ as an empirical constant whose value lies in the range $3 < \beta \leqslant 4$, one obtains good overall performance. We have also tried other transformation forms such as simple power functions and have obtained better results than simple subtraction-and-addition or multi-domain subdivision methods.

The success of this novel algorithm can be interpreted from two viewpoints. From a geometric point of view, the mapping (3.2) clusters points around the singularity while maintaining a regular spacing over the remainder of the integration interval. From a mathematical viewpoint, the variable mapping transforms the original singular integrand into a much more regular one where ordinary Gauss–Legendre quadrature can be applied with high accuracy. The nearly singular integrals which arise in close proximity to the collocation point have the form

$$I = \int_{-1}^{1} \frac{g(s)}{((s - s_0)^2 + d^2)^{m/2}} \mathrm{d}s, \tag{3.3}$$

where $s_0 \in (-1, 1)$, and are treated in a similar manner. The mapping variable is chosen in such a way that the singular point is removed from the interval of integration, but infinity is maintained at a respectful distance. Following the procedure by Muldowney & Higdon, the following transformation is used in our numerical scheme:

$$s = s_0 + d \sinh(n \sinh^{-1} \xi), \tag{3.4}$$

where the optimal choice of the parameter $n$ is the greatest integer satisfying

$$n \leqslant (1 + \ln \epsilon^{-1}), \tag{3.5}$$

$$\epsilon = d \quad \text{if} \quad |s_0| < 1, \qquad \epsilon = \min\{d, |s_0| - 1\} \quad \text{if} \quad |s_0| > 1. \tag{3.6}$$

While this variable transformation method is used for both the singular and nearly singular integrals, the adaptive Romberg quadrature is employed for the regular integrals. The local error is prescribed as $\epsilon = 10^{-6}$ in order to ensure adequate global accuracy. One finds that our method can successfully solve the integral equations (2.12) and (2.16) for high values of $\alpha$, i.e. a medium with closely spaced fibres.

## 4. Results and discussion of numerical results

### 4.1. *Convergence*

In order to demonstrate the reliability and accuracy of our method, we have performed a series of computations for simple particle motions in a Brinkman medium where there are known accurate results. All the numerical calculations were performed on a DECstation 3100. The computational time varied from several seconds to tens of minutes, depending on the number of surface elements used, the accuracy requirement for numerical evaluation of the integrals, and the value of the parameter $\alpha$ which characterizes the properties of the medium. We start with the pure translation of a sphere of radius $r_s$, whose analytic solution for drag is given by

$$F = 6\pi\mu U r_s \left(1 + \alpha + \tfrac{1}{9}\alpha^2\right) \tag{4.1}$$

Numerical results using 12, 24, 32 and 64 evenly distributed elements on the contour circle show relatively fast convergence to the exact results for all $\alpha$. The results using 32 elements and 64 elements differ by less than 0.2% and 0.1% from the exact solution (4.1), respectively. Using an error analysis similar to creeping flow, one can show that the discretization error in the present method is $O(\delta^2)$, where $\delta$ is the maximum size of the elements. The accuracy is further improved by using Richardson extrapolation for successive computations. We also calculated the drag on a disk translating edgewise using the boundary integral equation method. Comparison with the solution obtained by the dual integral equation method (Feng, Ganatos & Weinbaum 1998) shows very good agreement for $\alpha$ up to 50.

We next examined the translation of two spheres of the same radius $r_s$ and centre-to-centre spacing $2d$ moving perpendicular to their line of centres in a Brinkman medium (Kim & Russel 1985*a*). This motion is equivalent to a sphere translating parallel to a free surface, which will be discussed in detail in the next section, see figure 1(*b*). To the authors' knowledge, this is the only particle geometry other than a single sphere for which the Brinkman equation has been solved using either the method of reflections or the more accurate boundary collocation techniques developed by Gluckman *et al.* (1971). Unfortunately, Kim & Russel present graphical results rather than the detailed numerical results needed to rigorously evaluate the accuracy of the present technique. Thus, we first construct a solution using the original formulation of Gluckman *et al.* and then compare the results with those obtained by the present boundary integral equation method. This formulation is simpler but less versatile than the more robust method provided by Kim & Russel.

It can be shown that the multipole expansion of the general series solution of the Brinkman equation can be constructed from three auxiliary functions obtained by solving the Helmholtz equation (Kim & Russel 1985*a*). These auxiliary functions, representing the pressure field $p$, poloidal field $\Phi$ and toroidal field $\chi$, respectively, have simple forms in spherical coordinates. The velocity due to the translation of these

| | | $\alpha = 0$ | | $\alpha = 0.1$ | | $\alpha = 1.0$ | | $\alpha = 10.0$ | |
|---|---|---|---|---|---|---|---|---|---|
| $d/r_s$ | | $F_x$ | $T_y$ | $F_x$ | $T_y$ | $F_x$ | $T_y$ | $F_x$ | $T_y$ |
| 1.05 | (*a*) | 0.733 | $1.11 \times 10^{-1}$ | 0.765 | $1.26 \times 10^{-1}$ | 0.946 | $1.77 \times 10^{-1}$ | 1.082 | $4.64 \times 10^{-2}$ |
| | (*b*) | | | 0.769 | $1.29 \times 10^{-1}$ | 0.948 | $1.79 \times 10^{-1}$ | 1.084 | $4.66 \times 10^{-2}$ |
| 1.5 | (*a*) | 0.795 | $6.41 \times 10^{-2}$ | 0.838 | $7.21 \times 10^{-2}$ | 1.018 | $5.40 \times 10^{-2}$ | 1.023 | $1.19 \times 10^{-5}$ |
| | (*b*) | | | 0.839 | $7.24 \times 10^{-2}$ | 1.020 | $5.44 \times 10^{-2}$ | 1.024 | $1.21 \times 10^{-5}$ |
| 2.0 | (*a*) | 0.839 | $3.88 \times 10^{-2}$ | 0.889 | $4.27 \times 10^{-2}$ | 1.026 | $1.41 \times 10^{-2}$ | 1.008 | $2.86 \times 10^{-6}$ |
| | (*b*) | 0.839 | $3.89 \times 10^{-2}$ | 0.890 | $4.29 \times 10^{-2}$ | 1.027 | $1.43 \times 10^{-2}$ | 1.009 | $2.88 \times 10^{-6}$ |
| 3.0 | (*a*) | 0.888 | $1.84 \times 10^{-2}$ | 0.942 | $1.90 \times 10^{-2}$ | 1.012 | $1.16 \times 10^{-3}$ | 1.001 | $5.62 \times 10^{-7}$ |
| | (*b*) | 0.888 | $1.84 \times 10^{-2}$ | 0.942 | $1.91 \times 10^{-2}$ | 1.013 | $1.17 \times 10^{-3}$ | 1.001 | $5.64 \times 10^{-7}$ |
| 5.0 | (*a*) | 0.930 | $6.97 \times 10^{-3}$ | 0.982 | $5.98 \times 10^{-3}$ | 1.002 | $1.19 \times 10^{-5}$ | 1.000 | $7.32 \times 10^{-8}$ |
| | (*b*) | 0.930 | $6.98 \times 10^{-3}$ | 0.982 | $5.99 \times 10^{-3}$ | 1.002 | $1.21 \times 10^{-5}$ | 1.000 | $7.34 \times 10^{-8}$ |

TABLE 1. Comparison of the drag and torque coefficients normalized by the single-sphere result for two spheres moving perpendicular to their line of centres. (*a*) Results using the present boundary integral equation method with a total of 64 elements; (*b*) results using the exact solution of Goldman, Cox & Brenner (1966) for $\alpha = 0$, or results using the boundary collocation technique of Gluckman *et al.* (1971) described in the text with a total of 32 boundary collocation points for $\alpha \neq 0$.

two spheres $i = 1, 2$ can be expressed in terms of the following multipole expansion:

$$\boldsymbol{v} = \sum_{i=1}^{2} \left[ -\frac{1}{\mu\alpha^2} \nabla_i p_i + \nabla_i \times \nabla_i \times (\boldsymbol{x}_i \Phi_i) + \nabla_i \times (\boldsymbol{x}_i \chi_i) \right] \tag{4.2}$$

where

$$p_i = \sum_{n=1}^{\infty} a_{ni} r_i^{-n-1} P_n^1(\cos\theta_i) \sin\phi, \tag{4.3}$$

$$\Phi_i = \sum_{n=1}^{\infty} b_{ni} k_n(\alpha r_i) P_n^1(\cos\theta_i) \sin\phi, \tag{4.4}$$

$$\chi_i = \sum_{n=1}^{\infty} c_{ni} k_n(\alpha r_i) P_n^1(\cos\theta_i) \cos\phi, \tag{4.5}$$

where the modified spherical Bessel function of the second kind $k_n$ is defined by

$$k_n(x) = \left(\frac{\pi}{2x}\right)^{1/2} K_{n+1/2}(x). \tag{4.6}$$

The subscript $i = 1, 2$ means that the indicated quantities and operators are defined in a local coordinate system centred at the centre of the $i$th sphere, as shown in figure 1. The coefficients $a_{ni}$, $b_{ni}$ and $c_{ni}$ are determined by applying the boundary collocation technique. The drag and torque exerted on each sphere can be expressed as $2a_{11}/3$ and $c_{11}/\alpha^2$, respectively, after normalization by the single-sphere result (4.1) for the drag and the following expression for the torque (Solomentsev & Anderson 1996):

$$T = 8\pi\mu r_s^3 \Omega \frac{1 + \alpha + \frac{1}{3}\alpha^2}{1 + \alpha} \tag{4.7}$$

in which $\Omega$ is the angular velocity.

In solving equation (4.2) using the boundary collocation technique of Gluckman *et al.*, one satisfies the boundary conditions on the surface of each sphere at discrete

points evenly distributed on the contour. Since the resulting coefficient matrix will be singular if any of the collocation points are located on either the equator or at the poles, a small shift from these positions is made as discussed in Ganatos *et al.* (1982*a*) and Ganatos, Weinbaum & Pfeffer (1982*c*) in order to circumvent this difficulty. The calculation converges very rapidly as the number of collocation points is increased. These results are listed in table 1 along with the numerical results obtained by the present boundary integral equation method. In the present method, each of the sphere contours is divided into 32 line segments of equal length and further calculation using a larger number of elements has little influence on the convergence of the drag and torque coefficients. From table 1, we find that there is remarkably good agreement for both the drag and the torque coefficient even when the two spheres are close to each other, $d/r_s = 1.05$. It is also important to note that the torque exerted on each sphere is largely damped out by the intervening medium as $\alpha$ increases. Mathematically, this rapid decay in torque is due to $k_n(\alpha r_i)$, since $p_i$ does not contribute to the torque. This rapid decrease in torque indicates that confining boundaries or the other particles in the flow field will be significantly shielded by the medium at relatively small porosity. This shielding will be discussed further in the following sections.

### 4.2. *Results for translation of a sphere near a planar boundary*

In this section, we first consider the motion of a translating sphere of radius $r_s$ with velocity $U$ in the presence of a planar boundary in a fibre-filled medium with dimensionless permeability $\alpha$, as illustrated in figure 1($a, b$). The effective-medium approach and the boundary integral equation method formulated in the previous sections are used to obtain the solutions. The confining boundary can be either a solid wall on which the no-slip boundary condition must be observed or a planar free surface on which the shear stress vanishes. We only consider translation of the particle because for rotation the double layer contribution cannot be evaluated analytically and the computational expense will be tremendously increased. It is of particular interest to calculate the force and torque exerted on the sphere. These results will serve to demonstrate the combined effects of the surrounding fibres and the confining wall on the particle motion and reveal the hydrodynamic interactions in a fibre-filled medium.

Following established notation for Stokes flow, we express the drag and torque exerted on the sphere that translates perpendicular to a planar boundary with velocity $U$ in terms of dimensionless resistance coefficients which are normalized by either the Stokes results for an unbounded sphere, which reveal the combined effects of the fibrous medium and the confining boundary, or the Brinkman results for an unbounded sphere, which are suitable for inspecting the effect of the confining boundary in a Brinkman medium. Similarly, for parallel motion, the torque introduced by the presence of the wall will be normalized by either the Stokes torque on a rotating sphere in an infinite medium or result (4.7) for a sphere rotating in an unbounded Brinkman medium with angular velocity $U/r_s$.

For translation of a sphere toward a free surface, the flow field is equivalent to that generated by two spheres exhibiting mirror symmetry with respect to the free surface moving toward each other with equal velocity along their line of centres. In order to compare with the results obtained by the boundary integral method, we present an alternative solution procedure based on the multipole expansion method. Although one can construct the solution using the general solution (4.2) as was done for parallel motion, it is now convenient to introduce the stream function since the flow field is independent of the azimuthal angle $\phi$. Following Lawrence & Weinbaum (1986), we

express the stream function as

$$\psi = \sum_{i=1}^{2} \left[ \sum_{n=2}^{\infty} A_{ni} r_i^{-n+1} C_n^{-1/2}(\zeta_i) + \sum_{n=2}^{\infty} B_{ni} R_n(r_i) C_n^{-1/2}(\zeta_i) \right] \tag{4.8}$$

from which the fluid velocity components can be evaluated by

$$v_\sigma = \frac{1}{\sigma} \frac{\partial \psi}{\partial x}, \qquad v_x = -\frac{1}{\sigma} \frac{\partial \psi}{\partial \sigma}. \tag{4.9}$$

Here $C_n^{-1/2}(\zeta_i)$ are Gegnebauer function of degree $n$ with argument $\zeta = \cos\theta_i$ and $\theta_i$ is shown in figure 1($a$); $(\sigma, \phi, x)$ are corresponding cylindrical coordinates. The $R_n$ are polynomials in $1/r_i$, with an exponential multiplier, given by

$$R_n(r) = r^n \left( \frac{1}{r} \frac{\mathrm{d}}{\mathrm{d}r} \right)^{n-1} \frac{1}{r} \mathrm{e}^{-\alpha r} = r^{1/2} K_{n+1/2}(\alpha r). \tag{4.10}$$

The no-slip boundary conditions are applied on the surface of each sphere using the boundary collocation technique. Once the coefficients $A_{ni}$ and $B_{ni}$ are obtained, the drag on each of the spheres is obtained by the expression (Lawrence & Weinbaum 1986)

$$F_i = \alpha^2 (2\pi A_{2i} + V_p), \tag{4.11}$$

where $V_p$ is the particle volume. This expression can be used to check the accuracy of the more general boundary integral solution.

The geometry for both perpendicular and parallel motions can be obtained by rotating the contours $C_{pi}, i = 1, 2$ around the $x$-axis as indicated in figure 1. When the sphere moves perpendicular to the boundary, equation (2.12) is appropriate, whereas for parallel motion, equation (2.16) should be used instead. For parallel motion, we require that $u_x = 0$, $u_y = U$, $u_z = 0$ on the sphere surface, yielding $U_x = 0$, $U_\sigma = U_0$, $U_\phi = U_0$ for the Fourier components. On the solid wall, all velocity components vanish, whereas on the free surface, the derivatives of the velocity with respect to $x$ vanish. The standard boundary element method is used to discretize the resulting integral equation. More precisely, the sphere contour $C_{p1}$ is divided into straight line segments of equal length, whereas the semi-infinite confining walls $C_{p2}$ are truncated at various distances, $\sigma/r_s = 20$ or larger. Our numerical tests on these various truncations show that $\sigma/r_s = 30$ yields good convergence for both the drag and torque exerted on the sphere at all particle-to-wall spacings tested. The size of the wall elements is adjusted smaller in regions with large flow variation. The smallest wall element near the axis of symmetry is set equal to the size of the smallest element on the sphere surface, whereas the largest boundary element can be 20–30 times that of the smallest element adjacent to the axis of symmetry.

In figure 2 we plot the dimensionless resistance for a sphere translating perpendicular to a solid wall, normalized by the single-sphere result for either unbounded Stokes flow or the Brinkman medium. The figure shows the variation of the drag with respect to the relative particle–wall spacing $h/r_s$ for some representative values of $\alpha$, where $h$ denotes the distance from the centre of the sphere to the wall and equals $d$ as shown in figure 1. Figure 3 shows the corresponding results for a free surface. Comparison of the present results for $\alpha = 0$, i.e. Stokes flow, with the analytical solutions of Brenner (1961), indicates that the relative error lies within 0.1% for all spacings $h/r_s \geqslant 1.1$. This demonstrates the efficiency and accuracy of the present technique.

As mentioned above, the motion of a sphere in the presence of a free surface is

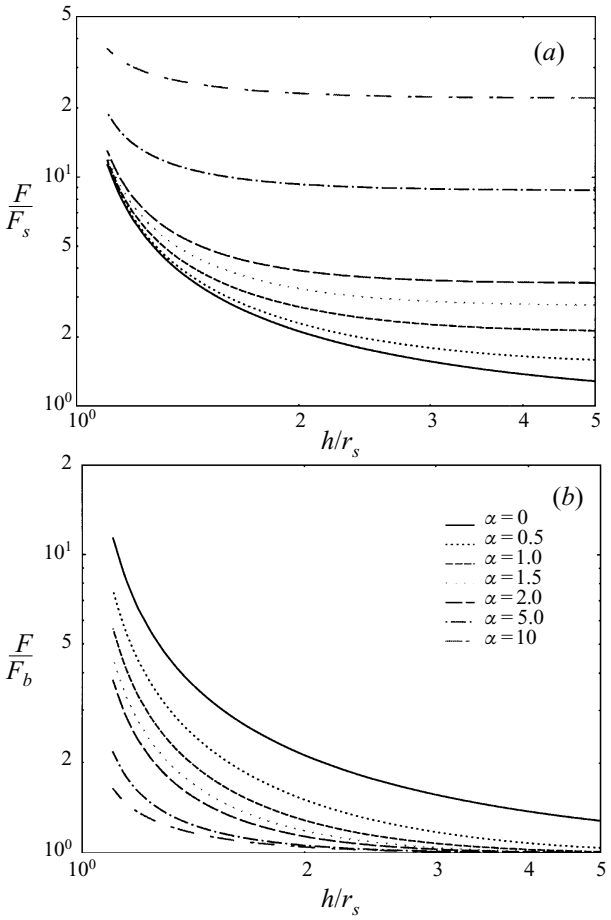


FIGURE 2. Normalized drag on a sphere moving perpendicular to a solid wall. (*a*) Results normalized by Stokes drag for a single sphere translating in an unbounded viscous fluid; (*b*) results normalized by drag for a single sphere translating in an unbounded Brinkman medium.

equivalent to the motion of two identical spheres with appropriate boundary conditions. Since this geometry also falls into the category in which the present technique can be applied, the results obtained by solving the integral equations numerically along $C_{p1}$ and $C_{p3}$ (see figure 1) can serve to eliminate the discretization and truncation errors due to the infinite extent of the planar boundary and further enables the solution to be obtained using velocity boundary conditions rather than their derivative. Comparison of the numerical results obtained by these two approaches and those calculated by equation (4.11) shows excellent agreement, with a relative difference less than 0.1%.

As the gap $h$ tends to zero, the dimensionless drag for both perpendicular and parallel motion exhibits certain singular behaviours. Surprisingly, the family of curves for small values of $\alpha$ seem to converge to the same value. From a physical viewpoint, the Brinkman equation describes the fluid motion on a length scale of $O(K_p^{1/2})$, or a fibre boundary layer of thickness $O(r_s/\alpha)$; therefore, the presence of a nearby planar wall will have a major influence on the flow field when $\alpha \leqslant O(1)$. Mathematically, there are two length scales involved in the motion of a particle near a wall in a

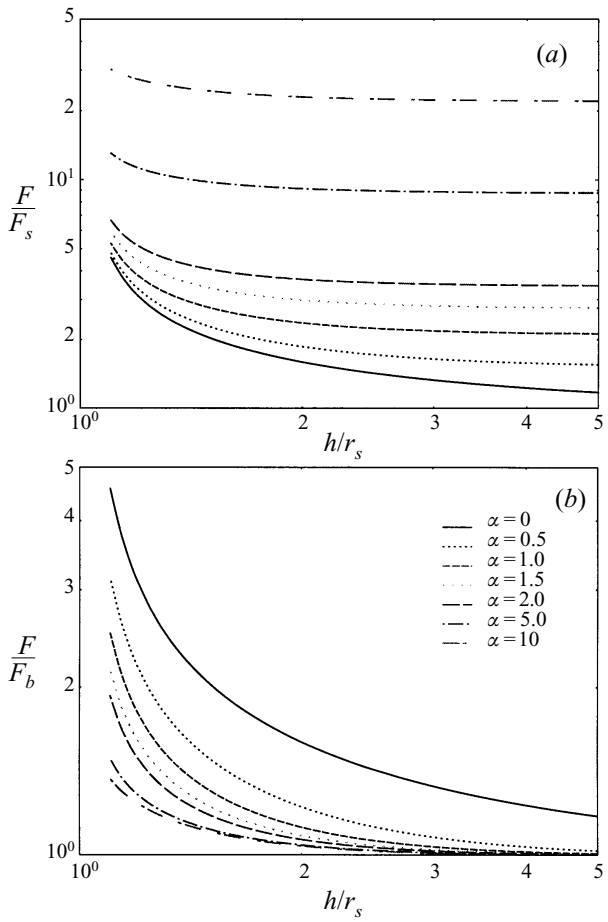


FIGURE 3. Normalized drag on a sphere moving perpendicular to a free surface. (*a*) Results normalized by Stokes drag for a single sphere translating in an unbounded viscous fluid; (*b*) results normalized by drag for a single sphere translating in an unbounded Brinkman medium.

Brinkman medium, the fibre boundary layer thickness and the particle–wall spacing. An asymptotic analysis using a multiple scaling technique is required to assess the relative importance of these two effects. In the Appendix, a local analysis indicates that the effect of the surrounding fibres is negligible compared to the effect of the confining boundary when $\alpha \leqslant O(1)$ and $\epsilon/r_s \leqslant O(1)$, where $\epsilon$ is the dimensionless gap width between the sphere and the boundary. Therefore, the well-known results for creeping flow are useful for this case. Comparing figure 2(*a*) and figure 3(*a*), one finds that for small values of $\alpha$, the effect of the confining boundary on the particle differs greatly depending upon whether the planar boundary is a free surface or a solid wall, as one would expect for Stokes flow. As $\alpha$ increases, the effect of the boundary is shielded by the surrounding fibres which now play a dominant role. The drags are essentially identical for the two cases for large values of $\alpha$ except in a very localized region near contact, see figures 2(*b*) and 3(*b*). In general, the solid wall retards the motion of the sphere more than a free surface for all $\alpha$.

As mentioned earlier, the motion of a sphere perpendicular to a planar boundary can be used as an idealized model to estimate the hydraulic resistance of a microvilli

tip as it penetrates the endothelial surface glycocalyx coating the exterior surface of the cell membrane. The minimum gap height between the microvilli and the membrane before receptor–ligand binding occurs is between 20 and 50 nm, leading to values of $h/r_s$ that range from 1.2 to 1.5 for microvilli of 100 nm diameter. If the fibre spacing is 7 nm and the fibre radius lies between 0.6 and 2 nm, the approximate formula (5.3), discussed in the next section, predicts that $\alpha$ lies in the range 18.8 to 23.6. Using the results for $\alpha = 10$ in figures 2(*a*) and 2(*b*), one concludes that the drag exerted by the glycocalyx will be much higher than the Stokes drag, and, although the effect of the membrane is greatly diminished by the surface glycocalyx, there is still a significant effect for $1.2 \leqslant h/r_s \leqslant 1.5$, see figures 2(*b*) and 3(*b*). Thus the present results indicate that the previous use of resistance functions based on Stokes flow is inappropriate for modelling the motion of microvilli in proximity to the endothelial surface. Detailed calculations for the local surface traction on the sphere indicate that the front half of the sphere encounters more than 70% of the total drag experienced by the particle for $h/r_s = 1.2$ and $\alpha = 1$, but that this differential decreases as $\alpha$ increases and $h/r_s$ decreases. A more realistic model for a microvilli is a hemisphere attached at the end of a circular cylinder. The hydrodynamic penetration force can be approximated by adding the resistance due to the longitudinal translation of a long cylinder in an unbounded medium and the resistance due to the front half of a sphere moving toward a planar boundary.

Figures 4(*a*) and 4(*b*) present the resistance coefficient for the parallel motion of a sphere adjacent to a plane, normalized respectively by the Stokes or Brinkman results for a sphere moving in an unbounded medium. One observes that the effect of the boundary on the sphere is much weaker than for perpendicular motion and exhibits new features not present for perpendicular motion. The drag on a sphere moving parallel to a free surface does not decrease monotonically with increasing distance from the boundary, although this is the case for parallel motion adjacent to a solid wall. The drag normalized by the Brinkman solution for an unbounded sphere can be smaller or larger than unity, indicating that the nearby free surface will either retard the motion of the sphere or enhance it depending on the relative distance from the free surface. This behaviour is the result of two competing effects. When $\alpha \leqslant O(1)$, which means that the porous medium is dilute, the far field Stokes interaction, which decays as $(O(1/r))$ is most important. In this case, due to the shear-free boundary condition on the surface, the fluid in the region between the sphere and the free surface moves along with the sphere rather than retarding its movement. Therefore, the resistance coefficient is smaller than one. On the other hand, when $\alpha$ increases, the resistance of the fibres dominates the motion and the fluid displaced in the near contact region contributes an additional resistance, which causes $F/F_b > 1.0$. The motion of a sphere parallel to a free surface is equivalent to two identical spheres moving perpendicular to their line of centres. When their centre-to-centre distance is sufficiently small, the fluid between the two spheres moves with the particles as if the sphere pair were enlarged, leading to a higher resistance. For intermediate values of $\alpha$, the competition between the fibre layer and the nearby boundary produces a more complicated behaviour for the drag and torque, as shown in figures 4 and 5. Figure 5 shows that the effect of the fibres on the torque is much weaker than their effect on the drag and that the torque has a maximum for $\alpha \geqslant 0.5$.

The results presented in figure 4(*a*, *b*) are most relevant for the lateral diffusion of molecules in the surface glycocalyx. Using formula (5.3), one finds that $\alpha$ for a molecule of 4 nm diameter varies between 0.75 and 0.94 for fibres of 0.6 to 2 nm radius when $\Delta = 7$ nm. For $\alpha$ in this range, the influence of the membrane can be

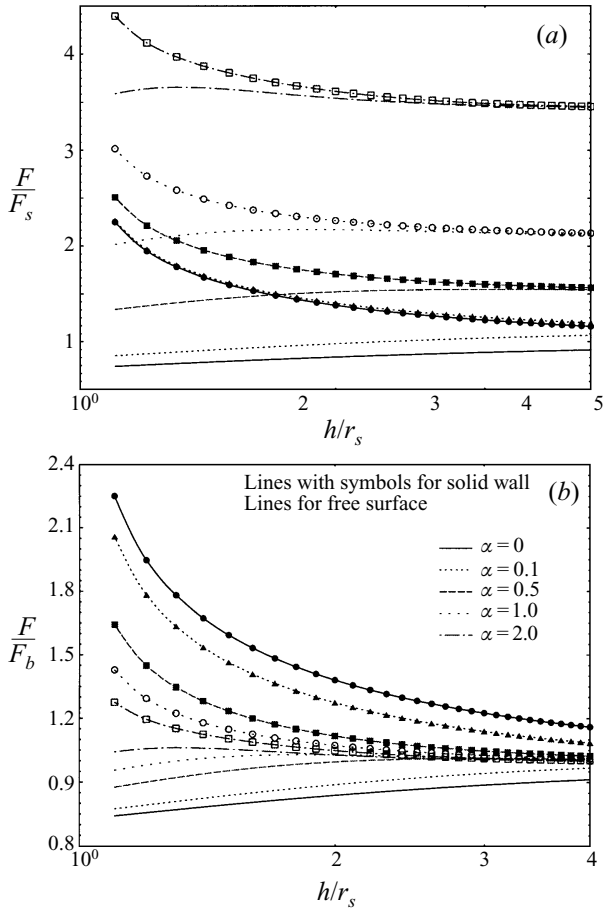


FIGURE 4. Normalized drag on a sphere moving parallel to a planar boundary. (*a*) Results normalized by Stokes drag for a single sphere translating in an unbounded viscous fluid; (*b*) results normalized by drag for a single sphere translating in an unbounded Brinkman medium.

considerable. For example, the membrane can cause a 45% increase in drag compared to an unbounded Brinkman medium for $\alpha = 1.0$ and $h/r_s = 1.1$. One also notes that there is about 50% more drag for motion near a solid wall than near a free surface when $h/r_s = 1.1$ and $\alpha = 1.0$. This difference diminishes as $h/r_s$ or $\alpha$ increases. In single particle tracking experiments, where 40 nm colloidal gold or 210 nm latex particles are used as tracers to study the cytoplasmic regulation of the movement of cell-to-cell adhesion molecules (Sako *et al.* 1998), the surface dynamics of transmembrane integrins (Schmidt *et al.* 1993) and the fence structure of the actin cytoskeleton (Sako & Kusumi 1995), the values of $\alpha$ greatly exceed those plotted in figure 4. Formula (5.3) predicts that $\alpha$ varies between 7.5 and 9.4 for the 40 nm gold particles and 39.4 and 49.5 for the 210 nm latex beads when $\Delta = 7$ nm and $0.6 < a < 2$ nm. For these values of $\alpha$ the drag is almost the same as for an unbounded Brinkman medium for either the solid or free surface boundary condition. Using the unbounded Brinkman expression for the drag and the Stokes–Einstein relation for the diffusion coefficient $D$, one estimates that $D$ for the 40 nm gold particle lies in the range $5.1 \times 10^{-9}$ cm$^2$ s$^{-1}$ to $7.2 \times 10^{-9}$ cm$^2$ s$^{-1}$ for the above values of $\alpha$. The experiments in Lee *et al.* (1993), which are based on the total resistance of the matrix, including elastic and

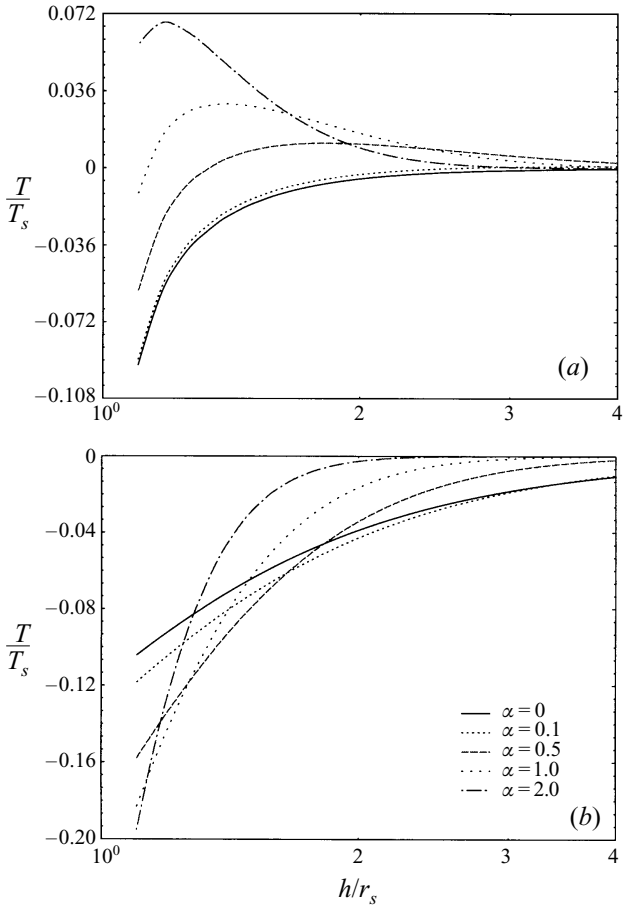


FIGURE 5. Torque on a sphere moving parallel to a planar boundary normalized by Stokes torque for a single sphere rotating in an unbounded viscous fluid: (*a*) solid wall, (*b*) free surface.

fibre binding energy, indicate that $D$ for the gold-tagged lipid molecule ranges from 1.1 to $1.7 \times 10^{-9}$ cm$^2$ s$^{-1}$. However, $D$ for the fluorescent-tagged molecule varies from 5.4 to $9.5 \times 10^{-9}$ cm$^2$ s$^{-1}$. The resistance of the lipid molecule in the membrane is thus about one-fifth of the gold-tagged lipid. Thus, the resistance of the gold particle is about 80% of the gold-tagged lipid and $D$ for the gold particle alone should range from 1.4 to $2.2 \times 10^{-9}$ cm$^2$ s$^{-1}$. This is approximately 30% of the value of $D$ predicted by the Brinkman equation, suggesting that 70% of the total resistance is associated with the elastic and binding energy of the surface glycocalyx.

### 4.3. *Results for translation of a sphere in a channel*

We next consider a sphere translating in a fibre-filled medium confined by a parallel walled channel of height $2H$, see figure 6. This geometry can be obtained by rotating the contours $C_{pi}, i = 1, 2, 3$ around the $x$-axis as indicated in the figure. The solution for this flow problem is obtained by solving the boundary integral equations (2.12) and (2.16) along $C_{pi}, i = 1, 2, 3$. The standard boundary element method is used to discretize the resulting integral equation, as described in detail in the previous subsection. Typical convergence tests on the normalized drag for parallel motion are presented in table 2 with increasing number of elements on the contours. As we

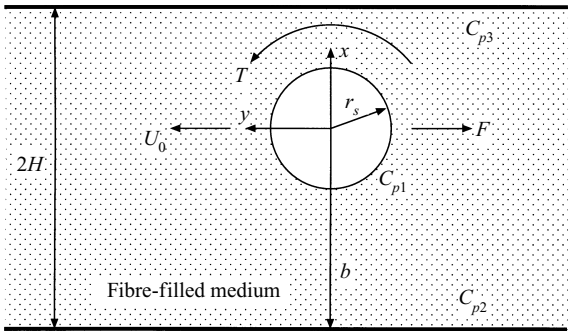


FIGURE 6. Geometry for a sphere moving in a channel.

(*a*) $\alpha = 0$

| Number of elements | $b/r_s = 2.5$ | $b/r_s = 2.0$ | $b/r_s = 1.5$ | $b/r_s = 1.2$ | $b/r_s = 1.1$ |
|---|---|---|---|---|---|
| 12/12/12 | 1.590 | 1.826 | 2.347 | 3.182 | 3.760 |
| 24/24/24 | 1.598 | 1.836 | 2.365 | 3.222 | 3.916 |
| 32/32/32 | 1.600 | 1.839 | 2.369 | 3.230 | 3.933 |
| 64/64/64 | 1.600 | 1.839 | 2.370 | 3.233 | 3.939 |
| Ganatos *et al.* | — | 1.846 | 2.377 | — | 3.94 |

(*b*) $\alpha = 1.0$

| Number of elements | $b/r_s = 2.5$ | $b/r_s = 2.0$ | $b/r_s = 1.5$ | $b/r_s = 1.2$ | $b/r_s = 1.1$ |
|---|---|---|---|---|---|
| 12/12/12 | 2.346 | 2.536 | 2.996 | 3.783 | 4.436 |
| 24/24/24 | 2.361 | 2.554 | 3.022 | 3.831 | 4.506 |
| 32/32/32 | 2.365 | 2.558 | 3.028 | 3.842 | 4.526 |
| 64/64/64 | 2.366 | 2.559 | 3.030 | 3.846 | 4.531 |

TABLE 2. Convergence of the normalized drag $F^t$ scaled by the Stokes drag $6\pi\mu U_0 r_s$ for a sphere translating along the centreline of a channel parallel to the walls.

can see in table 2(*a*), our results for $\alpha = 0$ agree closely with those obtained by the multipole collocation technique (Ganatos *et al.* 1980*a*) for the creeping motion of a sphere in a channel. The relative error is less than 0.5% for all values of $b/r_s$. For $\alpha = 1.0$, table 2(*b*), the number of boundary elements is increased until 0.5% convergence was achieved. This convergence test indicates that sufficiently accurate solutions can be achieved with 64 elements on each of the boundary contours for all possible types of motion.

We focus our attention on parallel motion. In figures 7 and 8 we have plotted the resistance coefficients for the drag and torque for a sphere translating in a parallel walled channel for various values of $\alpha$ and $H$. These coefficients are normalized by the drag and torque on a sphere translating or rotating in Stokes flow with the same translational or angular velocity. The results for the drag have the same qualitative behaviour as for Stokes flow. The results for the torque show that the direction of rotation, if the sphere were not held fixed, would change for a significant range of $b/H$. This phenomenon is also observed for a sphere translating in a channel in Stokes flow (Ganatos *et al.* 1980*a*). From these figures, we can conclude that the effect of the walls on the sphere is localized to the region near the walls for all $\alpha$. As the value of the parameter $\alpha$ increases, the effect of the wall becomes even smaller

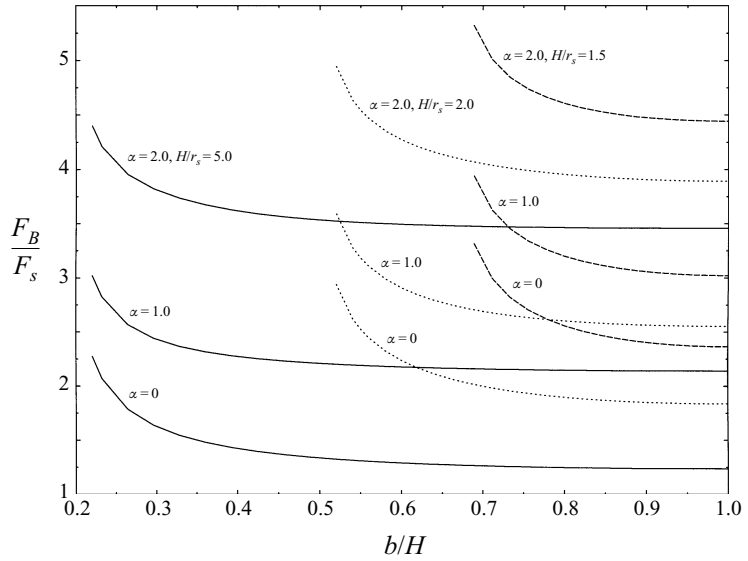


FIGURE 7. Normalized drag on a sphere moving in a channel for various channel half-heights, $H$, and representative values of $\alpha$. $F_s$ it the Stokes drag on a sphere in unbounded flow.

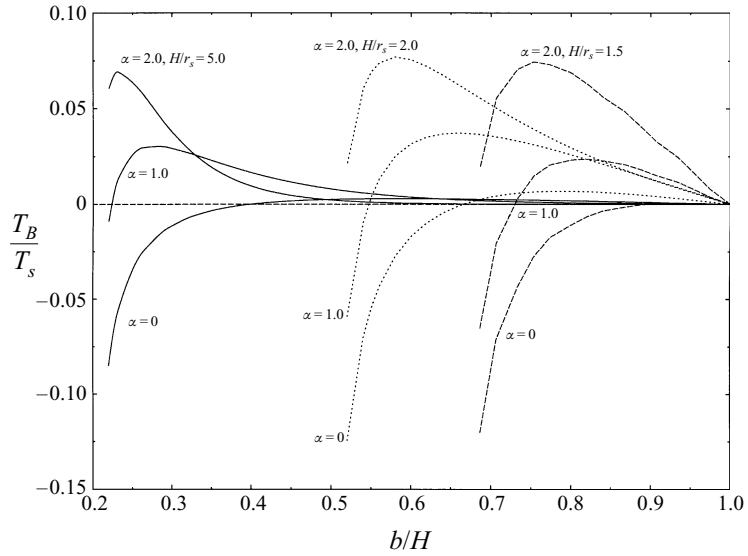


FIGURE 8. Normalized torque on a sphere moving in a channel for various channel half-heights, $H$, and representative values of $\alpha$. $T_s$ is the torque on a sphere rotating in unbounded Stokes flow.

as one would intuitively expect due to fibre shielding. In Stokes flow, we know the wall effect decays as $O(1/r)$, where $r$ is the distance from the boundary. However, in a fibre-filled medium, the effect of the confining boundaries is diminished by the presence of the fibres which shield the sphere from the wall. As $\alpha$ increases, the effect of the fibres dominates the drag and torque on the sphere even when the sphere is close to the wall. Therefore, the effect of the confining walls becomes less important for $\alpha \geqslant 2.0$. The corresponding results for the torque on the sphere exhibit a more complicated departure from the results for Stokes flow. As $\alpha$ increases, the torque

becomes exclusively positive. It is also evident that the torque coefficient has steep gradients in the proximity of the walls.

## 5. Application to transendothelial transport

In this section, numerical results presented in §4 are utilized to provide an improved model for determining the diffusion coefficient for the passage of spherical molecules through an interendothelial cleft filled with a fibre matrix. The continuum hydrodynamic theory used to calculate the phenomenological coefficients in the Kedem–Katchalsky equations derived from irreversible thermodynamics, will be extended to a Brinkman medium to account for particle–matrix interactions produced by the fibre components in the intercellular cleft between adjacent endothelial cells. In an earlier paper (Weinbaum *et al.* 1992), a new three-dimensional model was developed to elucidate some long-standing issues arising from attempts to relate the observed ultrastructural organization of the capillary interendothelial cleft and measured values for its permeability. A simple multiplicative formula was proposed to estimate the diffusive permeability of spherical solute molecules in an interendothelial cleft with cross-bridging cylindrical fibres.

We first wish to determine the permeability $K_p$ of the intercellular matrix. According to Darcy's law, the global permeability of the medium can be expressed as

$$\frac{Q}{A} = \frac{K_p}{\mu}\frac{\Delta p}{L}, \tag{5.1}$$

in which $Q$ is the volumetric flux rate through a cross-sectional area $A$ due to a pressure gradient over a length $L$ in the fibre-filled medium. Tsay & Weinbaum (1991) have examined the validity of the effective-medium approach by comparing the solution for the Stokes flow through a periodic square array of circular cylindrical fibres in a channel with the solution for the same channel flow using effective-medium theory. An empirical formula based on the extrapolation of the results for the two-dimensional drag coefficient was obtained for the case in which the height of the channel becames infinite. The following simple expression for the Darcy permeability was proposed:

$$K_p = 0.0572a^2\left(\frac{\Delta}{a}\right)^{2.377}, \tag{5.2}$$

where $a$ is the radius of the fibres and $\Delta$ is the open gap between two adjacent fibres in the periodic array. Equation (5.2) provides good agreement with the numerical solutions of Sangani & Acrivos (1982) for an infinite two-dimensional fibre array for all values of the fibre fraction $S$ in the range $0.001 \leqslant S < 0.7$. Using (5.2), one can express the dimensionless parameter $\alpha$ as

$$\alpha = 4.18\frac{r_s a^{0.189}}{\Delta^{1.189}}. \tag{5.3}$$

It is clear that the diameter of the spherical particle must be smaller than $\Delta$ for it to undergo Brownian motion in this periodic fibre array. This leads to a maximum allowable value $\alpha_{max}$ for a spherical particle of diameter $2r_s = \Delta$, namely,

$$\alpha_{max} = 2.09\left(\frac{a}{\Delta}\right)^{0.189}. \tag{5.4}$$

Two typical fibres that are believed to comprise the intercellular matrix are the sialyic

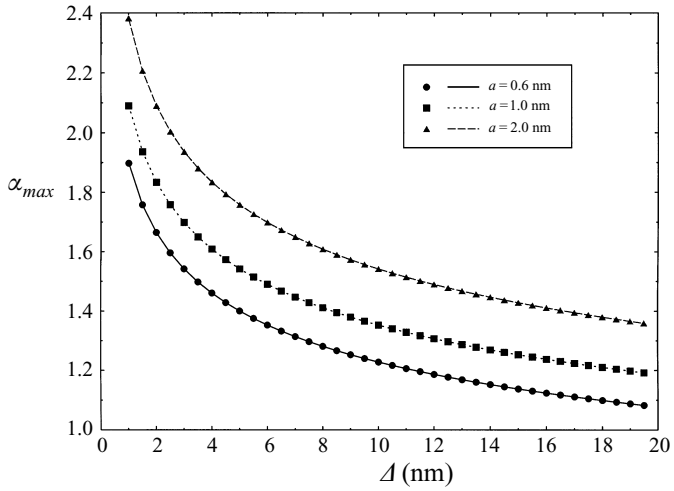


FIGURE 9. Variation of the maximum value of dimensionless permeability parameter $\alpha_{max}$ with respect to the gap between adjacent fibres for three different values of fibre radii.

side chains of proteoglycans, $a = 0.6$ nm radius, and their protein core, $a = 2$ nm radius. The variation of $\alpha_{max}$ with $\Delta$ is plotted in figure 9 for three fibre radii in this range. For $\Delta = 7$ nm, a fibre spacing that would allow only molecules smaller than albumin (diameter 7.2 nm) to pass, $\alpha_{max}$ lies between 1.30 and 1.65 for fibre radii between 0.6 and 2 nm. Subject to this constraint on $\alpha_{max}$, we shall now apply the effective-medium approach to estimate the diffusion coefficient for a spherical particle moving in a parallel walled channel.

The hydrodynamic force and torque on a translating spherical particle in a fibre-filled channel can be written as

$$F = 6\pi\mu r_s[UF_y^t + r_s\Omega F_z^r], \tag{5.5}$$

$$T = 8\pi\mu r_s^2[U\,T_y^t + r_s\Omega\,T_z^r], \tag{5.6}$$

where $F_y^t$, $T_z^t$ are the force and torque coefficients for the motion of a sphere due to a pure translation in the $y$-direction, while $F_y^r$ and $T_z^r$ are the corresponding coefficients due to a pure rotation about the $z$-axis, see figure 6. The balance between the hydrodynamic force and the gradient of the chemical potential on a neutrally buoyant, torque free particle yields

$$\frac{6\pi\mu r_s}{F(\alpha,\delta,s)}U = \frac{1}{N_A}\left[RT\frac{\mathrm{d}c}{\mathrm{d}x} + \bar{V}_s r_s\frac{\mathrm{d}P}{\mathrm{d}x}\right], \tag{5.7}$$

where

$$F(\alpha,\delta,s) = \frac{-T_z^r}{F_y^t T_z^r - F_z^r T_y^t}. \tag{5.8}$$

Here $c$ is the molar concentration, $\bar{V}_s$ is the molar volume, $N_A$ is Avogadro's number, $R$ is the universal gas constant, $T$ is the absolute temperature, and $\delta$ and $s$ are geometric parameters defined by $\delta = r_s/H$ and $s = b/2H$. As noted earlier, considerable computational effort is required to calculate the double layer potential in the boundary integral equation presented in § 4 for the pure rotation of a sphere. We notice, however, that the rate of growth of $F_y^t$ with respect to $\alpha$ is much faster than that of $T_y^t$. According to the Lorentz reciprocal theorem, the two coefficients $F_z^r$ and $T_y^t$ are related to each

other in the creeping limit as $3F_z^r = 4T_y^t$. Thus, a reasonable approximation to $F(\alpha, \delta, s)$ is

$$F(\alpha, \delta, s) \simeq -\frac{1}{F_y^t}. \tag{5.9}$$

Using a procedure proposed by Levitt (1975), one can write the diffusive permeability $\omega$ of the particle, after applying the conservation of flux through the cleft, as

$$\omega = \frac{L_p}{\bar{V}_s}\frac{2}{3}\delta^2(1-\delta)\bar{F}, \tag{5.10}$$

where

$$\bar{F}(\alpha, \delta) = \frac{2}{1-\alpha}\int_{r_s/2H}^{1/2} F(\alpha, \delta, s)\mathrm{d}s. \tag{5.11}$$

The left side of equation (5.7) is the drag force on the sphere. If we assume as a first approximation that all possible positions in the channel cross-section are equally likely, except the region of steric exclusion near the walls, then one can show that the mobility of the solute in the channel is given by $6\pi\mu r_s/\bar{F}(\alpha, \delta)$. If we now multiply (5.7) by $F(\alpha, \delta, s)/6\pi\mu r_s$, integrate across the channel height and notice that the ratio $R/N_A$ is just the Boltzman constant $k$, one can define the effective diffusion coefficient as

$$D_m = \bar{F}(\alpha, \delta)D_\infty, \tag{5.12}$$

where $D_\infty$ is the free diffusion coefficient from Stokes–Einstein theory for an infinite medium without a matrix.

The foregoing hydrodynamic theory does not include the effects of steric exclusion of the particle by the fibres and the spatial variation of the particle concentration in the available space of the fibre-filled medium. The steric exclusion contributes significantly to the diffusive permeability of the particle, especially when $r_s/a \sim 1$. In Weinbaum *et al.* (1992), a simple multiplicative formula was proposed to account for the combined effects of hydrodynamics and steric exclusion, namely that the effective diffusion coefficient could be written as

$$D_{eff} = D_m F(S), \tag{5.13}$$

where $D_m$ describes the hydrodynamic interaction and $F(S)$ the steric exclusion. The function $F(S)$ describes the diffusion of a point solute in the unbounded fibre array. The steric factor $S$ is defined by the excluded volume that is not accessible to the solute molecule. This same approach has also been adopted in Johnson *et al.* (1996) on the basis of hydrodynamic arguments proposed in Brady (1994).

Weinbaum *et al.* (1992) determined the steric factor $F(S)$ by solving the solute diffusion equation for a doubly periodic fibre array in which the zero flux boundary condition is imposed at the exclusion radius, $r_e = r_s + a$. Therefore, steric exclusion is treated as a geometric restriction in which the center of the particle cannot enter a region within a distance less than $r_s$ from the fibre surface. Equivalently, the fibre radius is augmented by the particle radius. Using (5.13) and this solution for the steric function $F(S)$, one obtains

$$D_{eff} = D_m\left(\frac{1-b_1S_e}{1+b_1S_e}\right), \tag{5.14}$$

where $b_1$ is a constant representing the flow configuration and depends only on the

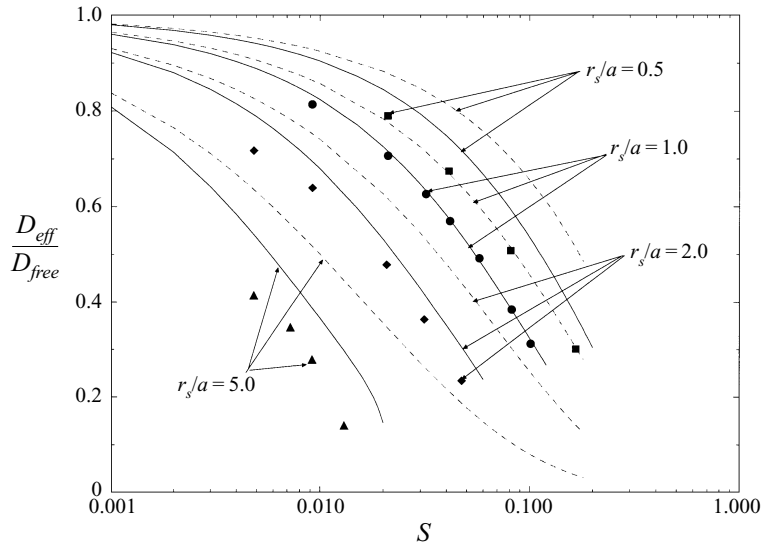


FIGURE 10. Comparison of the normalized diffusion coefficient obtained by a simple multiplicative formula (5.14), solid lines, and data points (symbols) obtained using Stokesian dynamics simulation for a sphere moving in an unbounded fibre-filled medium. Also shown, dashed lines, are the results for effective-medium theory without the steric exclusion factor $F(S)$ in (5.14).

effective fibre solid fraction $S_e = S(1 + r_s/a)^2$ and is given in figure 5 of Weinbaum *et al.* (1992). It decreases rapidly with increasing effective solid fraction $S_e$.

To test the applicability of the simple approximation (5.14), we first examine the diffusion of a solute molecule of radius $r_s$ in an unbounded square array of parallel fibres of radius $a$. This same problem has been rigorously treated using generalized Taylor dispersion theory and a Stokesian dynamic simulation in which the fibres are described by a bead and string model (Phillips *et al.* 1990). This comparison is shown in figure 10. In the effective-medium approach one uses the Brinkman solution for the motion of a sphere in an unbounded medium (4.1) to calculate $D_m$. Also shown in the figure are the results predicted by the effective-medium theory without the steric correction factor in (5.14). It is clear that the steric correction provided by the simple multiplicative formula (5.14) provides a substantial improvement, especially for values of $r_s/a \neq 1$.

To examine the diffusion of a solute molecule in a channel filled with a Brinkman medium, $D_m$ given by equation (5.12) has been plotted in figure 11. One notes that the effect of the walls, the departure from the solution for $H = \infty$, is most significant for small values of $\alpha$, i.e. low fibre fractions. For $\alpha > 1.0$, the effect of the fibres becomes more important than the walls for $H > 5$, while for $\alpha > 1.65$ the wall effect is greatly damped by fibre shielding. However, as shown in figure 9, depending on the fibre spacing parameter $\Delta$, particle trapping may have already occurred and values of $\alpha > 2$ may not be achievable. In general, the presence of the confining walls reduces the diffusion coefficient and is a significant effect for $H < 2$ for all $\alpha \leqslant \alpha_{max}$ in figure 9.

We have also plotted in figure 11, dashed lines, the simple multiplicative formula proposed in Weinbaum *et al.* (1992) for $D_m$ in which the hydrodynamic effects of the fibres and the walls are treated separately, i.e. the expression for $D_m$ in (5.12) is

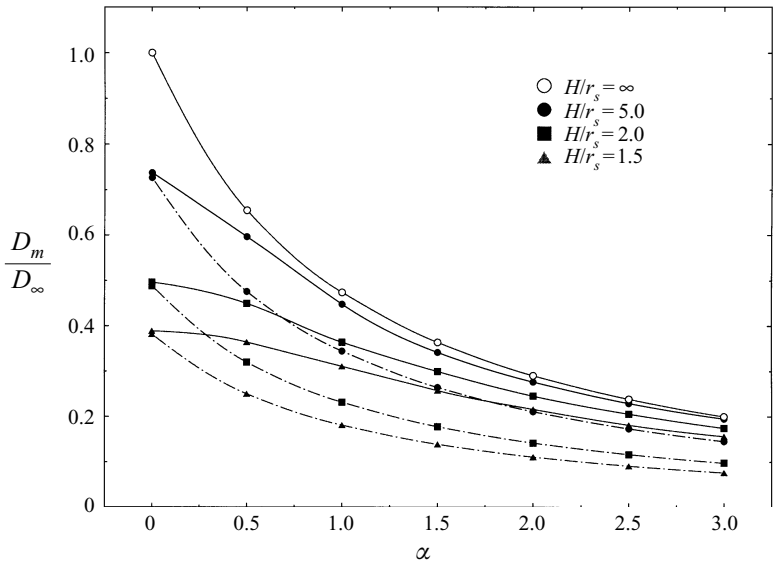


FIGURE 11. Comparison of the normalized diffusion coefficient obtained by the present numerical method (5.12)(solid lines), and simple multiplicative formula (5.15)(dashed-dot lines), for a sphere diffusing in a fibre-filled channel of various channel half-heights $H$.

approximated by

$$D_m = D_{iw}\left(1 + \alpha + \frac{\alpha^2}{9}\right)^{-1}, \tag{5.15}$$

where $D_{iw}$ is the diffusion coefficient for a sphere in a parallel walled channel in Stokes flow (Ganatos *et al.* 1980*b*), and the second factor is the added resistance due to the motion of a sphere in an unbounded Brinkman medium, see equation (4.1). We see that the presence of the fibres leads to a substantial increase in the diffusion coefficient beyond the value of predicted by (5.15). This increase in $D_m$ results from the shielding of the wall by the fibres surrounding the diffusing solute molecule. One notes that the agreement of (5.15) with the present numerical results is good only for either small $\alpha$, where the effect of the wall dominates, or large $\alpha$ and large $H$, where the fibres completely shield the particle from the walls. The discrepancy for intermediate values of $\alpha$ is substantial for all values of the channel half-height $H$.

Finally, in figure 12, we have plotted the normalized effective diffusion coefficient, scaled by the diffusion coefficient $D_{b\infty}$ for an infinite Brinkman medium, for two different fibre radii when the gap between fibres is 7 nm. At this fibre spacing all molecules larger than albumin would be sieved. Figure 12 shows the combined effects of the walls and the steric exclusion factor in equation (5.14). For a fine fibre of radius 0.6 nm, for which $\alpha_{max}$ increases linearly with $r_s$ up to $\alpha_{max} = 1.3$, $D_{eff}/D_{b\infty}$ decreases rapidly as $r_s$ increases. As $r_s$ approaches $\Delta/2$, the steric correction $F(S)$ becomes more important than the hydrodynamic interaction. For the larger fibres of 2 nm radius, for which $\alpha_{max} = 1.7$, the hydrodynamic drag on the solute is 20% to 25% larger than for the 0.6 nm radius fibres. The steric exclusion factor $F(S)$ is also smaller since the exclusion radius $r_e$ will be larger for the same value of $r_s$. In general, the combined effects of hydrodynamic wall interaction and steric exclusion result in a significantly lower diffusion coefficient than a solute molecule diffusing in an unbounded Brinkman medium with the same value of $\alpha$. These results are

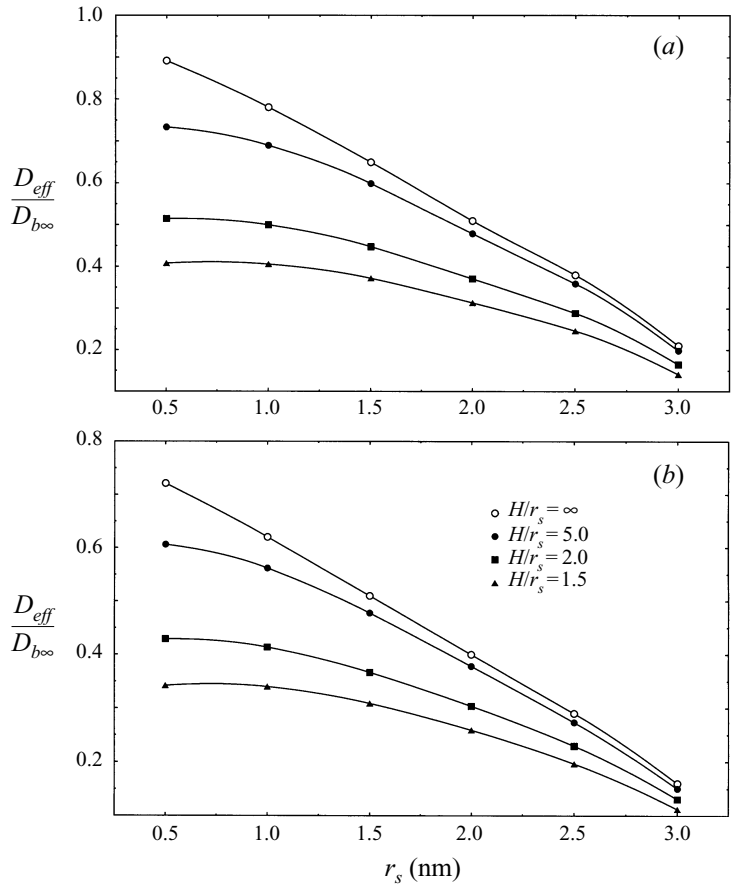


FIGURE 12. Normalized diffusion coefficient obtained by the present numerical method for a sphere of radius $r_s$ diffusing in a fibre-filled medium in a channel of various channel half-heights $H$ including the steric correction for a periodic fibre array given by equation (5.14). $\Delta = 7$ nm and (*a*) $a = 0.6$ nm, (*b*) $a = 2$ nm. $D_{b\infty}$ is the Brinkman result for an infinite medium without the steric correction function $F(S)$.

particularly useful in evaluating current studies of the structure-function relationship for solutes diffusing through interendothelial clefts (Weinbaum *et al.* 1992; Fu *et al.* 1994).

## 6. Concluding remarks

In summary, this paper has developed a general numerical approach to the solution of the Brinkman equation describing particle motion in a fibre-filled medium with confining walls. Although the present technique is capable of solving the governing equations for any value of $\alpha$, there is a maximum allowable value for a given fibre structure if a diffusing particle is not to exceed the open clearance between two adjacent fibres. In many biological problems which involve particle diffusion in a fibre-filled medium, this maximum value of $\alpha$ lies in the range 1.2 to 1.7. The hydrodynamic effect of the fibres surrounding the particle will significantly diminish the effect of confining boundaries or other particles when $\alpha > 1.0$. Since the torque on a rotating sphere due to a confining boundary is a lower-order effect than the drag,

we are able to neglect particle rotation in our simplified theory for the diffusion of a spherical solute molecule in a parallel walled channel. The results in § 5 show that this assumption is also acceptable in the small-$\alpha$ limit, Stokes flow. This approximate theory shows that the simple multiplicative formula proposed in Weinbaum *et al.* (1992), where the contribution from the walls and the fibres are treated separately, underpredicts the solute diffusion coefficient.

The boundary integral equation method developed in this paper takes advantage of the symmetry of the flow geometry to reduce the problem to a system of one-dimensional integral equations defined on the contours of the particle and the boundaries. An efficient numerical algorithm for evaluating the singular integrals, based on the procedure proposed by Muldowney & Higdon (1995) for Stokes flow is extended to the Brinkman equation. It is demonstrated that the present method is both efficient and accurate, even for large values of $\alpha$. However, when we consider the general motion of the particle, such as rotation or the presence of a non-uniform upstream flow, the much more complicated contribution of the double layer integral in (2.8) cannot be simply evaluated as in Stokes flow. Thus the computational efforts will be substantially increased, especially for flows with infinite boundaries, in which a large number of boundary elements are required when the integral equation is discretized. The present method can be readily extended despite these limitations. For example, the axisymmetric motion of sphere in a cylinder filled with a Brinkman medium or the motion of a sphere across the centreline of a circular orifice or the entrance of a circular tube of finite length, can all be investigated using the present method. Since the Brinkman equation is analogous to the unsteady Stokes equation, one can utilize the present method to solve the axial oscillation of an axisymmetric particle at high frequency, a problem for which most earlier techniques will fail.

This study has been performed in partial fulfillment of the requirements for the PhD degree of J. Feng from the Graduate School and University Center of the City University of New York. Financial support from NIH grant HL 44485 is gratefully acknowledged.

## Appendix

In this Appendix, we will show that the leading term for the motion of a sphere near a planar boundary is independent of the permeability parameter $\alpha$ if $\alpha \sim O(1)$ and $\epsilon = \delta/r_s = h/r_s - 1$, the dimensionless gap height, is $< O(1)$. The procedure is an extension to that used for creeping flow (Jeffrey 1982; O'Neill & Stewartson 1967). Another approach is given by Goldman, Cox & Brenner (1967) for the motion of a sphere parallel to a plane wall.

For axisymmetric motion perpendicular to an infinite planar boundary, the flow is axisymmetric and it is convenient to introduce the dimensionless stream function which satisfies

$$E^2(E^2 - \alpha^2)\psi = 0. \tag{A 1}$$

Introducing two stretched variables

$$R = \epsilon^{-1/2}\sigma, \qquad X = \epsilon^{-1}x, \tag{A 2}$$

the governing equation becomes

$$\left[\frac{\partial^2}{\partial X^2} + \epsilon\left(\frac{\partial^2}{\partial R^2} - \frac{1}{R}\frac{\partial}{\partial R}\right)\right]\left[\frac{\partial^2}{\partial X^2} + \epsilon\left(\frac{\partial^2}{\partial R^2} - \frac{1}{R}\frac{\partial}{\partial R}\right) - \epsilon^2\alpha^2\right]\psi = 0. \tag{A 3}$$

The boundary condition on the sphere surface in the near contact region is given by

$$\psi = -U_0\sigma^2/2 = -\epsilon R^2/2. \tag{A 4}$$

Thus we expand the stream function $\psi$ as

$$\psi = r_s^2\epsilon(\psi_0 + \epsilon\psi_1 + \cdots) \tag{A 5}$$

and on substitution into (A 3), we obtain a hierarchy of equations,

$$\frac{\partial^4\psi_0}{\partial X^4} = 0, \qquad \frac{\partial^4\psi_1}{\partial X^4} = -2\Theta\frac{\partial^2\psi_0}{\partial X^2}, \ \cdots \tag{A 6}$$

for $\alpha = O(1)$ and

$$\frac{\partial^2}{\partial X^2}\left(\frac{\partial^2}{\partial X^2} - \beta^2\right)\psi_0 = 0, \tag{A 7}$$

$$\frac{\partial^2}{\partial X^2}\left(\frac{\partial^2}{\partial X^2} - \beta^2\right)\psi_1 = -2\Theta\frac{\partial^2\psi_0}{\partial X^2} + \beta^2\Theta\psi_0, \tag{A 8}$$

for $\alpha = \epsilon^{-1}\beta$ and $\beta = O(1)$ where the operator $\Theta = \partial^2/\partial R^2 - (1/R)\partial/\partial R$. The boundary conditions for $\psi_i$ are obtained by a Taylor expansion at $X = 1 + R^2/2$. Notice that for $\alpha = O(1)$, the regular expansion of $\psi$ is identical to that for creeping flow.

Now consider a sphere of unit radius moving parallel to a planar solid wall. Due to the axisymmetric flow configuration, the pressure $p = \mu P(\sigma, x)\cos\phi$. The momentum equation when expressed in terms of the velocity components ($U\cos\phi, V\sin\phi, W\cos\phi$) can be written in cylindrical coordinates $(\sigma, \phi, x)$ as

$$\frac{\partial P}{\partial\sigma} = \mathrm{L}_0^2 U - \frac{2(U+V)}{\sigma^2} - \alpha^2 U, \tag{A 9}$$

$$-\frac{P}{\sigma} = \mathrm{L}_0^2 V - \frac{2(U+V)}{\sigma^2} - \alpha^2 V, \tag{A 10}$$

$$\frac{\partial P}{\partial x} = \mathrm{L}_1^2 W - \alpha^2 W, \tag{A 11}$$

and the continuity equation becomes

$$\frac{\partial U}{\partial\sigma} + \frac{U+V}{\sigma} + \frac{\partial W}{\partial z} = 0, \tag{A 12}$$

where the operator $\mathrm{L}_m^2$ is defined by

$$\mathrm{L}_m^2 \equiv \frac{\partial^2}{\partial\sigma^2} + \frac{1}{\sigma}\frac{\partial}{\partial\sigma} - \frac{m^2}{\sigma^2} + \frac{\partial^2}{\partial x^2}. \tag{A 13}$$

Introducing the stretched coordinates $X$ and $R$ as defined in (A 2), the boundary conditions on the sphere surface together with the continuity equation suggest expansions of the pressure velocity components in the form

$$P = \epsilon^{-3/2}P_0(R, X) + \epsilon^{-1/2}P_1(R, X) + \cdots, \tag{A 14}$$

$$U = U_0(R, X) + \epsilon U_1(R, X) + \cdots, \tag{A 15}$$

$$V = V_0(R, X) + \epsilon V_1(R, X) + \cdots, \tag{A 16}$$

$$W = \epsilon^{1/2}W_0(R, X) + \epsilon^{3/2}W_1(R, X) + \cdots. \tag{A 17}$$

Substitution of the asymptotic expansions into the governing equations leads to a

hierarchy of equations, of which the leading order for $\boldsymbol{U}_0$ and $P_0$ is either

$$\frac{\partial P_0}{\partial R} = \frac{\partial^2 U_0}{\partial X^2}, \tag{A 18}$$

$$-\frac{P_0}{R} = \frac{\partial^2 V_0}{\partial X^2}, \tag{A 19}$$

$$\frac{\partial P_0}{\partial X} = 0, \tag{A 20}$$

$$\frac{\partial U_0}{\partial R} + \frac{U_0 + V_0}{2} + \frac{\partial W_0}{\partial X} = 0 \tag{A 21}$$

for $\alpha = O(1)$ or

$$\frac{\partial P_0}{\partial R} = \frac{\partial^2 U_0}{\partial X^2} - \beta^2 U_0, \tag{A 22}$$

$$-\frac{P_0}{R} = \frac{\partial^2 V_0}{\partial X^2} - \beta^2 V_0, \tag{A 23}$$

$$\frac{\partial P_0}{\partial X} = 0, \tag{A 24}$$

$$\frac{\partial U_0}{\partial R} + \frac{U_0 + V_0}{2} + \frac{\partial W_0}{\partial X} = 0 \tag{A 25}$$

for $\alpha = \beta\epsilon^{-1}$ and $\beta \sim O(1)$, provided that $\alpha \leqslant O(\epsilon^{-1})$. Note that equations (A 18)–(A 21) are exactly the same as for creeping flow.

The new parameter $\beta$ defined by $\alpha\epsilon$ can be estimated using the empirical formula

$$\beta = 4.18 \left(\frac{a}{\delta}\right)^{0.189} \left(\frac{\delta}{\Delta}\right)^{1.189}, \tag{A 26}$$

derived from equation (5.3), where $\delta$ is the dimensional gap height. When $\beta = O(1)$ the minimum gap between the sphere and the confining wall is comparable with fibre spacing. We anticipate that in this case, the contribution from the surrounding fibres to the drag is as important as that from the boundary.

Comparison with the numerical results for $\epsilon = 0.05, 0.1$ indicates that the following additive formula for the drag provides a good approximation for $\alpha \leqslant 2.0$ for both perpendicular and parallel motions:

$$\frac{F}{6\pi\mu r_s U_0} = \left(1 + \alpha + \frac{\alpha^2}{9}\right) + F_{Stokes}, \tag{A 27}$$

where $F_{Stokes}$ is the asymptotic drag for a sphere moving close to a planar boundary in Stokes flow.

## REFERENCES


Adamson, R. H. & Clough, G. 1992 Plasma proteins modify the endothelial cell glycocalyx of frog mesenteric microvessels. *J. Physiol.* (*Lond.*) **445**, 473–486.

Alon, R., Chen, S., Puri, K. D., Finger, E. B. & Springer, T. A. 1997 The kinetics of L-selectin tethers and the mechanics of selectin-mediated rolling. *J. Cell Biol.* **138**, 1169–1180.

Brady, J. F. 1994 *Hindered Diffusion.* In *Extended Abstracts, AIChE Annual Meeting*, San Fransisco, CA, p. 320.

Brenner, H. 1961 The slow motion of a sphere through a viscous fluid towards a plane surface. *Chem. Engng Sci.* **16**, 242–251.

Brinkman, H. C. 1947 A calculation of the viscous force exerted by a flowing fluid in a dense swarm of particles. *Appl. Sci. Res.* A **1**, 27–34.

Bruehl, R. E., Springer, T. A. & Bainton, D. F. 1996 Quantitation of L-selectin distribution on human leukocyte microvilli by immunogold labeling and electron microscopy. *J. Histochem. Cytochem.* **44**, 835–844.

Durlofsky, L. & Brady, J. F. 1987 Analysis of the Brinkman equation as a model for flow in porous media. *Phys. Fluids* **30**, 3329–3341.

Feng, J., Ganatos, P. & Weinbaum, S. 1998 The general motion of a circular disk in a Brinkman medium. *Phys. Fluids* **10**, 2137–2146.

Fu, B. M., Curry, F. E. & Weinbaum, S. 1994 A junction-orifice-entrance layer model for capillary permeability: application to frog mesenteric capillary. *Trans. ASME: J. Biomech. Engng* **116**, 502–513.

Ganatos, P., Pfeffer, R. & Weinbaum, S. 1980*a* A strong interaction theory for the creeping motion of a sphere between plane parallel boundaries. Part 2. Parallel motion. *J. Fluid Mech.* **99**, 755–783.

Ganatos, P., Weinbaum, S., Fischbarg, J. & Liebovich, L. 1980*b* A hydrodynamic theory for determining the membrane coefficients for the passage of spherical molecules through an intercellular cleft. *Adv. Bioengng, ASME* **3**, 193–196.

Ganatos, P., Weinbaum, S. & Pfeffer, R. 1980*c* A strong interaction theory for the creeping motion of a sphere between plane parallel boundaries. Part 1. Perpendicular motion. *J. Fluid Mech.* **99**, 739–753.

Gluckman, M. J., Pfeffer, R. & Weinbaum, S. 1971 A new technique for treating multi-particle slow viscous flow: axisymmetric flow past spheres and spheroids. *J. Fluid Mech.* **50**, 705–740.

Goldman, A. J., Cox, R. G. & Brenner, H. 1966 The slow motion of two identical arbitrarily oriented spheres through a viscous fluid. *Chem. Engng Sci.* **21**, 1151–1170.

Goldman, A. J., Cox, R. G. & Brenner, H. 1967 Slow viscous motion of a sphere parallel to a plane wall. I. Motion through a quiescent fluid. *Chem. Engng Sci.* **22**, 637–652.

Howells, I. D. 1974 Drag due to the motion of a Newtonian fluid through a sparse random array of small fixed rigid objects. *J. Fluid Mech.* **64**, 449–475.

Hsu, R. & Ganatos, P. 1989 The motion of a rigid body in viscous fluid bounded by a plane wall. *J. Fluid Mech.* **207**, 29–72.

Huang, Y., Rumschitzki, D., Chien, S. & Weinbaum, S. 1994 A fibre matrix model for the growth of macromolecular leakage spots in the arterial intima. *Trans. ASME: J. Biomech. Engng* **116**, 430–445.

Jeffrey, D. J. 1982 Low-Reynolds-number flow between converging spheres. *Mathematika* **29**, 58–66.

Johnson, E. M., Berk, D. A., Jain, R. K. & Deen, W. M. 1996 Hindered diffusion in agarose gels: test of effective medium model. *Biophys. J.* **70**, 1017–1126.

Kim, S. & Karrila, S. J. 1991 *Microhydrodynamics: Principles and Selected Applications.* Butterworth-Heinemann.

Kim, S. & Russel, W. B. 1985*a* The hydrodynamic interactions between two spheres in a Brink-man medium. *J. Fluid Mech.* **154**, 253–268.

Kim, S. & Russel, W. B. 1985*b* Modeling of the porous media by renormalization of the Stokes equations. *J. Fluid Mech.* **154**, 269–286.

Kosar, T. F. & Phillips, R. J. 1995 Measurement of protein diffusion in dextrans solutions by holographic interferometry. *AIChE J.* **41,** 701–711.

Lawrence, C. J. & Weinbaum, S. 1986 The force on an axisymmetric body in linearized, time-dependent motion: a new memory term. *J. Fluid Mech.* **171**, 209–218.

Lee, G. M., Zhang, F., Ishihara., A, McNeil, C. L. & Jacobson, K. A. 1993 Unconfined lateral diffusion and and estimate of pericellular matrix viscosity revealed by measuring the mobility of gold-tagged lipids. *J. Cell Biol.* **120**, 25–35.

Levitt, D. J. 1975 General continuum analysis of transport through pores I. proof of Onsager's reciprocity postulate for uniform pore. *Biophys. J.* **15**, 533–551.

Loewenberg, M. 1994 Axisymmetric unsteady Stokes flow past an oscillating finite-length cylinder. *J. Fluid Mech.* **265**, 265–288.

Lundgren, T. S. 1972 Slow flow through stationary random beds and suspensions of spheres. *J. Fluid Mech.* **51**, 273–299.

Muldowney, G. P. & Higdon, J. J. L. 1995 A spectral boundary element approach to three-dimensional Stokes flow. *J. Fluid Mech.* **298**, 167–192.

O'Neill, M. E. & Stewartson, K. 1967 On the slow motion of a sphere parallel to a nearby wall. *J. Fluid Mech.* **27**, 705–724.

Phillips, R. J., Deen, W. M. & Brady, J. F. 1989 Hindered transport of spherical macromolecules in fibrous membranes and gels. *AIChE J.* **35**, 1761–1769.

Phillips, R. J., Deen, W. M. & Brady, J. F. 1990 Hindered transport in fibrous membranes and gels: effect of solute size and fibre configuration. *J. Colloid Interface Sci.* **139**, 363–379.

Pozrikidis, C. 1988 A study of linearized oscillatory flow past particles by the boundary-integral method. *J. Fluid Mech.* **202**, 17–41.

Pozrikidis, C. 1992 *Boundary Integral and Singularity Method for Linearized Viscous Flow*. Cambridge University Press.

Pozrikidis, C. 1994 The motion of particles in the Hele–Shaw cell. *J. Fluid Mech.* **261**, 199–222.

Sako, Y. & Kusumi, A. 1995 Barriers for lateral diffusion of transferrin receptors in the plasma membranes as characterized by receptor dragging by laser tweezers: fence versus tether. *J. Cell Biol.* **129**, 1559–1574.

Sako, Y., Nagafuchi, A., Tsukita, S., Takeichi, M. & Kusumi, A. 1998 Cytoplasmic regulation of the movement of E-cadherin on the free cell surface as studied by optical tweezers and single particle tracking: corraling and techering by the membrane skeleton. *J. Cell Biol.* **140**, 1227–1240.

Sangani, A. S. & Acrivos, A. 1982 Slow flow past periodic arrays of cylinders with application to heat transfer. *Intl J. Multiphase Flow* **8**, 193–206.

Schmidt, C. E., Horwitz, A. F., Lauffenburger, D. A. & Sheetz, M. P. 1993 Integrin cytoskeletal interactions in migrating fibroblasts are dynamic, asymmetric, and regulated. *J. Cell Biol.* **123**, 977–991.

Solomentsev, Y. E. & Anderson, J. L. 1996 Rotation of a sphere in Brinkman fluids. *Phys. Fluids* **8**, 1119–1121.

Tam, C. K. W. 1969 The drag on a cloud of spherical particles in low Reynolds number flow. *J. Fluid Mech.* **38**, 537–546.

Tsay, R. & Weinbaum, S. 1991 Viscous flow in a channel with periodic cross-bridging fibres: exact solutions and Brinkman approximation. *J. Fluid Mech.* **226**, 125–148.

Vink, H. & Duling, B. R. 1996 Identification of distinct luminal domains for macromolecules, erythrocytes and leukocytes within mammalian capillaries. *Circ. Res.* **71**, 581–589.

Weinbaum, S. 1998 Models to solve mysteries in biomechanics at the cellular level; a new view of fibre matrix layers. *Ann. Biomed. Engng* **26**, 1–17.

Weinbaum, S., Ganatos, P. & Yan, Z. Y. 1990 Numerical multipole and boundary integral equation techniques in Stokes flow. *Ann. Rev. Fluid Mech.* **22**, 275–316.

Weinbaum, S., Tsay, R. & Curry, R. E. 1992 A three-dimensional junction-pore-matrix model for capillary permeability. *Microvascular Res.* **44**, 85–111.

Youngren, G. K. & Acrivos, A. 1975 Stokes flow past a particle of arbitrary shape: a numerical method of solution. *J. Fluid Mech.* **69**, 377–403.